We are IntechOpen, the world's leading publisher of Open Access books Built by scientists, for scientists

6,900
Open access books available

185,000
International authors and editors

200M
Downloads

Our authors are among the

154
Countries delivered to

TOP 1%
most cited scientists

12.2%
Contributors from top 500 universities



WEB OF SCIENCE™

Selection of our books indexed in the Book Citation Index in Web of Science™ Core Collection (BKCI)

Interested in publishing with us?
Contact book.department@intechopen.com

Numbers displayed above are based on latest data collected.
For more information visit www.intechopen.com



Chapter 9

Mg-Based Thin Films as Model Systems in the Search for Optimal Hydrogen Storage Materials

Małgorzata Norek

Additional information is available at the end of the chapter

http://dx.doi.org/10.5772/48261

1. Introduction

There is a growing necessity of reducing greenhouse gases emissions to the atmosphere. A renewable energy system based on the use of electricity and hydrogen as energy carriers does not result in harmful pollutants being released to the natural environment. Hydrogen and fuels cells satisfy all requirements for an environmentally friendly vehicle. However, on-board hydrogen storage remains a key problem. It still remains to understand better the mechanisms involved in the interaction of hydrogen with matter. The search of an optimal storage material is a complicated process, were an interplay of many variables need to be considered.

In recent years, magnesium hydride (MgH_2) has attracted considerable attention as hydrogen storage material because of its large gravimetric density of 7.7 wt%, reversible hydrogen storage and low cost. The research has been focused on improving poor hydrogen sorption kinetics and lowering high dissociation temperature (~ 673 K). Strategies to reduce the stability of MgH_2 include alloying with various elements and nanostructuring. It was shown that mechanical ball milling can reduce particle size up to ~10 nm, introduce defects, large surface areas, and grain boundaries and in turn decrease the strength of the metal-hydrogen bond. Milling with different catalysts has improved noticeably hydrogen sorption kinetics.

Although the ultimate goal is the production of large amounts of hydrogen storing materials to be used in the transport sector, thin film processing is an alternative method that provides the opportunity to synthesize nanostructured materials in specific compositions, well-defined microstructures and dimensions. This, in turn, offers the possibility of more rational approach to the problem which might contribute to progress in hydrogen technology. Upon

INTECH
open science | open minds

© 2012 Norek, licensee InTech. This is an open access chapter distributed under the terms of the Creative Commons Attribution License (http://creativecommons.org/licenses/by/3.0), which permits unrestricted use, distribution, and reproduction in any medium, provided the original work is properly cited.

the size reduction to the nanoscale, the analysis of the finite-size effects, such as: surface or interface contributions to the hydrogenation thermodynamics and quantum-size effects, is possible. Moreover, cooperative phenomena (elastic interaction within the interfacial region) can be introduced through the synthesis of multilayer films and kinetic limitations can be minimized, leading to novel materials with unique properties. Thin films do not suffer as much from embrittlement and/or decrepitation as bulk materials, allowing to study cyclic absorption and desorption. Buckling of the film due to hydrogen loading occurs when the elastic energy stored in the film exceeds the adhesion energy. In case of weak adhesive forces between the film and the substrate the mechanical stress generated during the hydride formation relaxes by a buckle-and-cracks network formation. If the stress is high, but the adhesion still strong enough to hinder detachment of the film, the film will remain intact but the stress relaxes via plastic deformations (e. g. dislocations etc.). As a result of the dominant elastic out of plane expansion of a strongly clamped film, the morphology of the film does not alter. Thanks to a well-defined structure, composition and dimension of thin films, the thin film approach allows to study: the reaction pathways, the role of catalysts, the phase segregation and diffusion phenomena occurring during hydrogen absorption and release, which are of great importance in the rational design of the hydrogen storage materials for practical applications.

The chapter will briefly review the techniques and methods used to investigate the interaction of hydrogen with matter. Next, the hydrogen properties of Pd-capped Mg thin films will be presented. The most important achievements in the research of the Mg-based alloy thin films will be described in detail. Alloying Mg with small quantity of 3d transition metals (Sc, Ti, V, Cr, Ni, Fe, Cu, Co) can tailor the hydrogen reaction enthalpy and consequently reduce the operating temperatures during hydrogen absorption and desorption. High-throughput screening methods have allowed to select many promising Mg-based alloys with specific chemical compositions which are characterized by very good kinetics and high hydrogen capacity.

2. Methods and measurements

The techniques applied to research the hydrogen interaction with matter in bulk materials are usually not applicable in thin films. Classical methods such as volumetric and gravimetric techniques, in which the hydrogen is measured via the pressure drop or by the increased weight of the sample, are difficult to apply to thin films due to the small quantities of hydrogen involved. Hydrogen concentration within the thin films can be measured by: electrochemical loading, nuclear reaction analysis (NRA), elastic recoil detection analysis (ERDA), or neutron reflectivity (NR) [1].

In the electrochemical loading the metal film is used as a negative electrode. The electrochemical reaction corresponds to the reduction of water and involves one electron per absorbed hydrogen atom. As a result of the reaction hydrogenation of the thin film occurs. For a material able to absorb a quantity of hydrogen C_{sg} by solid–gas reaction, an equivalent electrochemical capacity, C_{el}, can be calculated according to the Equation:

$$C_{el}(mAh/g) = \frac{C_{sg}F}{3.6M} \quad (1)$$

where F is the Faraday constant, C_{sg} is expressed in H atoms per formula unit (H/f.u.), and M is the molecular weight of the alloy in g/f.u. [2].

The ion beam analytical methods, such as NRA or ERDA, are nondestructive, straightforward and completely quantitative. The high accuracy of the techniques is mainly due to the precision with which cross-sections of the involved atomic and nuclear processes are known. During the bombardment the interaction of the particle beam with a material (elastic and inelastic scattering, nuclear reactions and electromagnetic excitation) takes place. The material composition can be deduced from the number of observed events per incident beam particle.

In NRA, the ion beams of MeV (up to ~50 MeV) is applied for materials analysis. When the light projectiles impinge on light to medium heavy atoms, nuclear reactions in the target nuclei can occur. The yield of the reaction products (γ, p, n, d, ^{3}He, ^{4}He, etc.) is proportional to the concentration of the specific elements in the sample. Absolute concentrations can be calculated easily with the help of simple standards (e.g. bulk material or compounds of the analyzed elements). NRA is most often applied for the analysis of H, Li, Be, B, C, N, O, F, Na, Al, P with detection limits range from 10^{-3} to 10^{-7}. Reactions with narrow resonances (100 eV to 1 keV) can be found for many of the aforementioned elements. By stepping up the accelerator energy and thus shifting the depth (d) within the target at which the reaction takes place, the depth profiling with a resolution of the order of 10 nm is measured (Figure 1).

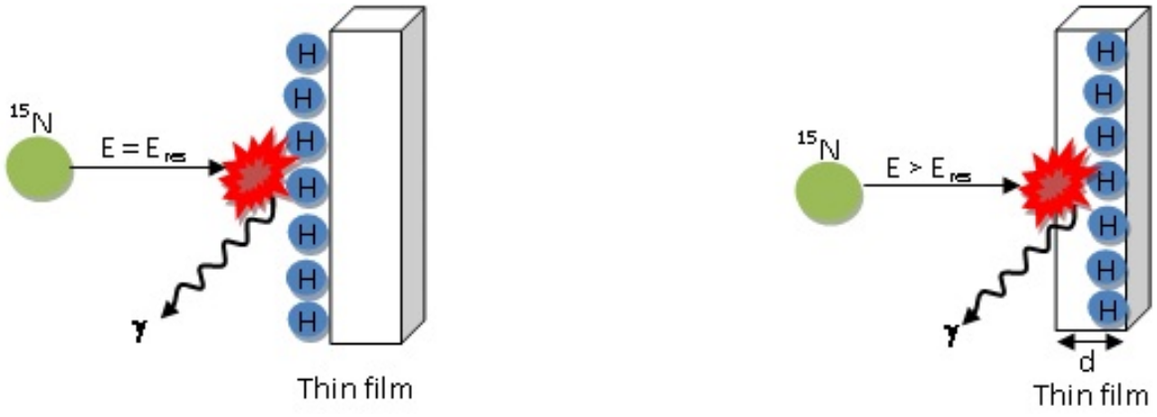


Figure 1. A scheme of hydrogen depth profiling with the ^{15}N ions.

Within the film the ^{15}N ions are slow down to the resonant energy E = 6.4 MeV and react with hydrogen according to the formula: ^{1}H(^{15}N,^{12}C)$\alpha\gamma$. The detected number of γ quants, of a characteristic energy of 4.965 MeV, is proportional to the hydrogen concentration at a certain depth.

ERDA is one of the few fully quantitative hydrogen profiling methods. Elements lighter than the incident beam particles (2 MeV ^{4}He beam for hydrogen detection) are analyzed (e.g.

hydrogen profiling) by detection of the recoiling target atoms in a grazing angle geometry (Figure 2). Absorber foils or mass discriminating detectors are used in order to discriminate between forward scattered projectiles and different types of recoiling particles. The depth profiles of all light target elements can be obtained simultaneously well separated from each other.

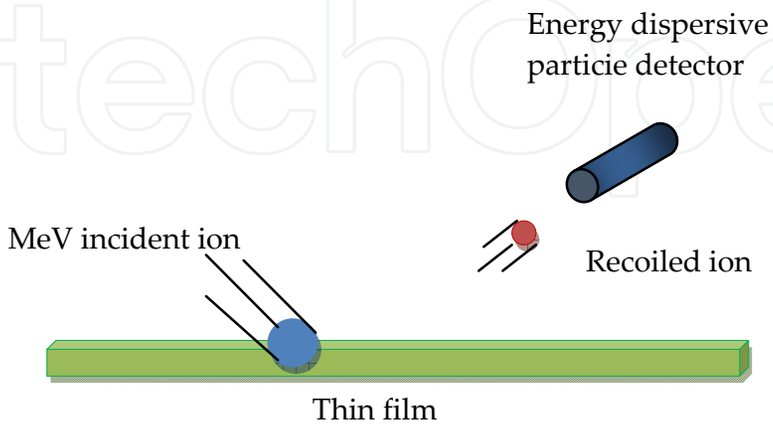


Figure 2. A scheme for ERDA experiment

Neutron reflectivity (NR) method is based on the fact the neutrons obey the same laws as electromagnetic waves and as such display reaction and refraction on passing from one medium to another. The sample is exposed to a beam of neutrons and the reflectivity is measured as a function of the momentum transfer q. A specular reflectivity experiment measures the scattered intensity as a function of $q_z = 2k_z$ (perpendicular to the interface). As such, the reflectometry experiment provides information about structure perpendicular to the interface. For specular reflection (the reflection which is defined as reflection in which the angle of reflection equals the angle of incidence, Figure 3) the critical angle is given by Equation 2:

$$\theta_C = \lambda\sqrt{\frac{\delta}{\pi}} \tag{2}$$

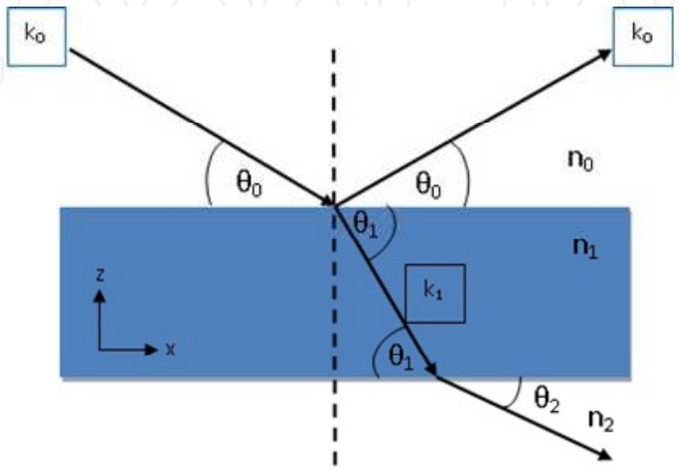
where λ is the neutron wavelength 4.75 Å, δ is the scattering length density, which is defined by the Equation 3:

$$\delta = \frac{\Sigma_i^n b_i}{V} \tag{3}$$

where b_i is the scattering length of the relevant atom and V is the volume containing the n atoms [3]. The hydrogen concentration can be, thus, calculated directly from a measure of the critical angle [4].

There are many indirect methods exploiting hydrogen induced changes of other physical properties of the film. The hydrogen uptake has often been monitored by measuring the

sample resistance. To study the hydrogen loading and the thermodynamic properties four point probe measurement is commonly used [5]. Under applied hydrogen pressure at constant temperature, the resistance of metal thin film increases due to a decrease in electron mobility with H acting as scattering centers. Also the changes of the elastic, the magnetic and the optical propertied could be used to follow the hydrogen uptake. The conversion to hydrogen concentrations must then be carried out by another independent calibration measurement.



$$k_z = k_0 \sin\theta_0$$

$$q_z = 2k_z = 4\pi/\lambda \sin\theta_0$$

Figure 3. A thin film of refractive index n_1 between two bulk media of refractive indices n_0, n_2.

Thin films open new fields of research such as screening for new composite materials. Matrix samples or samples with defined chemical composition allow the simultaneous investigation of hydrogen sorption by means of combinatorial approaches. Two of them rely on changes in the optical response, as measured by the emissivity in the IR, or the optical transmission in the visible region, during the change from the metal to hydride, or hydride to metal, phase. The third one is carried out by X-ray microdiffraction, a sequential characterization which aimed at identification of structural phases rather the decomposition temperatures and storage capacities.

IR screening technique is based on the change of the apparent temperature due to the surface emissivity variations. According to Stefan-Boltzmann law (Eq. 4) the radiation power of the material is proportional to its emissivity (ε):

$$W = \sigma \varepsilon T^4 \tag{4}$$

Emissivity, in turn, depends on the resistivity of the material (ρ), as defined by the Hagen-Rubens low (Eq. 5):

$$\varepsilon = 2(2\varepsilon_0 \omega \rho)^{1/2} \tag{5}$$

Since metal hydrides are characterized by higher resistivity than their corresponding pure metals, it is possible to measure hydrogenation/dehydrogenation process by monitoring the emissivity of a given material. During the measurement a large part of the radiation emitted by the material is partially reabsorbed by the atmosphere either inside or outside the chamber where the experiment is being performed and is reflected by the IR camera lenses. Thus, the apparatus measures in fact the effective radiation (*W'*) which is automatically converted into an apparent temperature (T_a) [6]:

$$T_a = \left(\frac{W'}{\sigma}\right)^{1/4} = T(\varepsilon)^{1/4} \tag{6}$$

The metal thin film blocks IR radiation and appears black in the IR camera. Upon hydrogenation the material becomes optically transparent and the IR camera will see the bright region at the point where the hydride is forming. The IR screening method was introduced by Olk [7, 8]. Oguchi et.al used the method, combined with structural characterization, to determine the rate of a hydride phase growth [9]. Although the hydrogen content cannot be quantify directly, the IR screening is a valuable tool for studying the kinetics of the hydrogen sorption or fast identification of catalyst.

The method based on the change of optical transmission upon hydrogen loading is called "Hydrogenography" and was developed by Gremaud and coworkers [10]. The amount of light transmitted through a thin film is measured by means of a 3CCD camera as a function of hydrogen pressure at constant temperature. Moreover, the optical transmission can be related to the hydrogen concentration via Lambert-Beer's law [11]. Therefore, the hydrogenography allows for a detailed quantitative study of both kinetics and the thermodynamics of hydrogenation/dehydrogenation process. The concentration depends linearly with the logarithm of the optical transmission T [12]:

$$\ln\left(\frac{T}{T_0}\right) \propto c \tag{7}$$

Pressure vs. $\ln(T/T_0)$ isotherms (PTI's which are equivalent to the standard PCI's) of thousands of different samples can be measured simultaneously. Based on these measurements performed at various temperatures Van't Hoff plots can be built and the thermodynamic parameters, such as enthalpy of the hydrogen-induced phase transitions, can be determined (Figure 4). An advantage of the method is that it can works equally for both materials which perform the metal-to-insulator transition upon hydrogen uptake and for materials which remain metallic after the process [13]. The stresses associated with the clamping of a thin film to a substrate must be taken, however, into account when transferring the experimental data to bulk samples.

The other combinatorial methods which make use of the stresses was developed by Ludwig and coworkers [14]. Thin films are deposited onto the array of 24 Si cantilevers and are exposed to H_2 gas. As a result of the in-plane stresses and out-of-plain strains induced by

the volume expansion occurring during the H_2 loading, the bending of the cantilevers takes place. The cantilever bending is monitored by an optical approach: a laser diode beam is split into parallel lines by the optics and the lines are projected on the cantilevers. The individual reflections from each cantilever are projected on a semitransparent screen and are recorded by CCD camera (Figure 5).

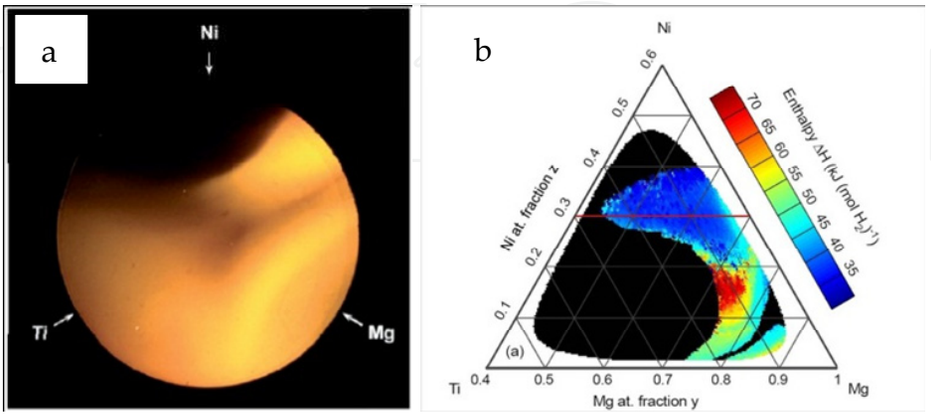


Figure 4. a) Optical transmission image of a $Mg_yNi_zTi_{1-y-z}$ gradient film during loading at 333K and b) Hydride formation enthalpies of the Mg-Ni-Ti-H system, determined from the Van't Hoff plots for each pixel of the $Mg_yNi_zTi_{1-y-z}$ gradient film (from Ref. [10]).

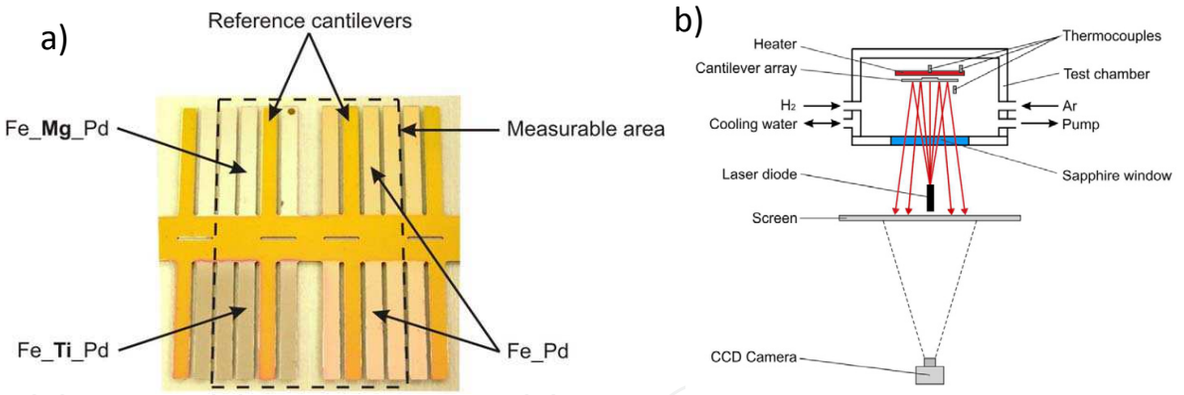


Figure 5. a) A cantilever material library: 24 cantilevers are arranged in 4 quadrates, 16 cantilevers are simultaneously observable; uncoated cantilevers serve as reference, b) schematic of the gas phase apparatus (from Ref. [14]).

The method was successfully applied to Mg-Ni system: the hydrogen induced stress was correlated with the composition and microstructure of the films [15]. Similar technique based on measurement of the surface curvature of a dense array of 2500 MEMS-fabricated cantilevers was developed by Woo et al. [16].

A different screening method was presented by Guerin and coworkers [17]. The technique uses a silicon microfabricated MEMS array with 49 heaters, independently controllable, which allow both temperature programmed desorption and infrared thermography measurements. The integrals of the TPD (Temperature Programmed Desorption) provide a direct measure of the hydrogen storage capacity as a function of composition. Due to the

application of high heating rates to detect hydrogen with sufficient sensitivity, the measurements are performed far away from the equilibrium conditions. Therefore, the method is complementary to the techniques which allow for the determination of thermodynamic parameters.

3. Pd-capped Mg thin films

Hydride uptake by metal is governed by a thermodynamic process as described by pressure – concentration isotherm (Figure 6) [18]. At the beginning of the process the host metal dissolves some portion of hydrogen to form solid state solution (α-phase). Upon the H concentration increase in the metal, the H-H interaction become dominant and the nucleation of the hydride (β-phase) occurs. The region where the two phases coexist (the plateau pressure in the isotherm) defines the amount of hydrogen that can be stored reversibly at a given pressure and temperature. The H content decreases with increasing H_2 pressure and temperature [19]. The equilibrium pressure, p_{eq}, (the plateau pressure) depends strongly on the temperature. The relation is expressed by the Van't Hoff equation (Eq. 8):

$$\ln\left(\frac{p_{eq}}{p_{eq}^{0}}\right)=\left(-\frac{\Delta H}{R}\right)\left(\frac{1}{T}\right)+\frac{\Delta S}{R} \tag{8}$$

where R is the gas constant, the ΔH and the ΔS are the changes of enthalpy and entropy, respectively, and $p_{eq}^{0} = 1.013 \times 10^5$ Pa is the standard pressure. Thus, the slope of the van't Hoff curve determines the enthalpy, whereas the intercept gives the values of the entropy of the process.

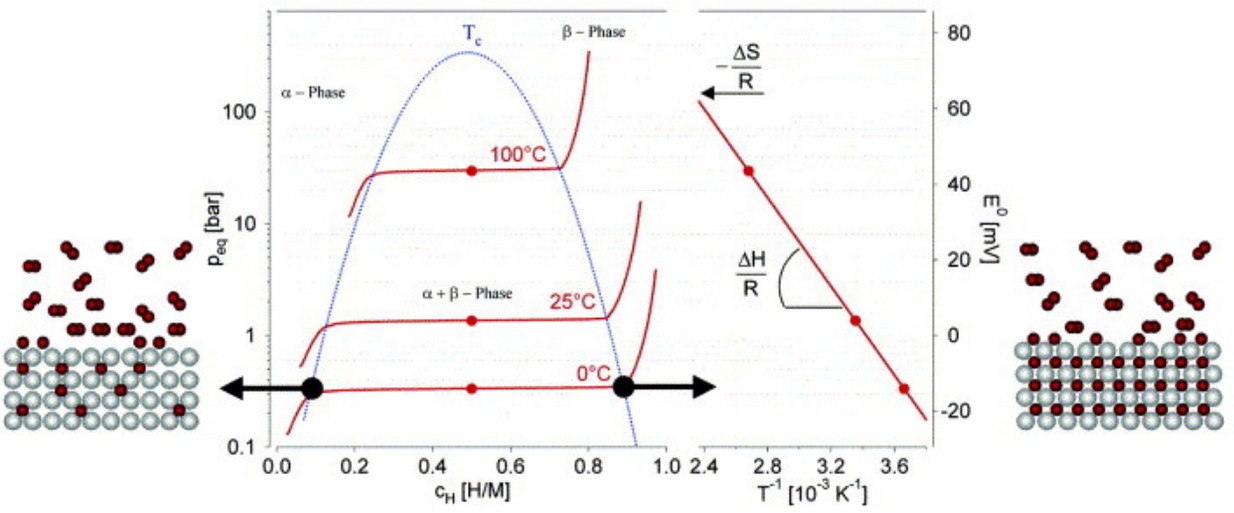


Figure 6. Pressure-concentration-temperature plot and a van't Hoff curve (logarithm of the equilibrium or plateau pressure vs. the reciprocal temperature) for an intermetallic compound (from Ref. [18]).

MgH_2 decomposes into Mg bulk and H_2 gas, the reaction being endothermic (ΔH>0), while the reaction of the formation of MgH_2 from Mg bulk and H_2 gas is exothermic (ΔH<0). The

value of the enthalpy for MgH_2 formation/decomposition is ~ 75 kJ/mol, which means that at ambient pressure (~1 bar) the operating temperature is of ca. 600K [20, 21]. This is much too high for the practical application. It is not easy to lower the enthalpy of hydrogenation (or dehydrogenation) process since it involves the binding energy between the hydrogen atom and a metal. Recent DFT and HF calculations made for the Mg/MgH_2 system clearly show that considerable changes in the thermochemistry of hydrogen absorption/desorption can be achieved only if the particle size is reduced below 2 nm. A steep decrease in the enthalpy of MgH_2 formation was found within the ultrasmall MgH_2 particle region (0.62-0.92 nm) [22]. The desorption enthalpies were calculated to be -20.64, 34.54, and 61.86 kJ/mol H_2 for the MgH_2 nanowires with diameter of: 0.68 nm, 0.85 nm, and 1.24 nm, which were derived from the Mg nanowires with diameter of 0.32 nm, 0.71 nm, and 1.04 nm, respectively (Figure 7) [23]. The phenomena was explained by the fact that in the case of such an extreme downsizing the vast majority of Mg and H atoms are exposed to the surface, where hydrogen atoms occupy the less stable top and bridges sites. In larger crystals the hydrogen resides in the more stable, three-coordinate sites. Consequently, surface Mg atoms are left uncoordinated and the hydrogen atoms are more easily absorbed/desorbed from these energetically less favored sites. The same trend was observed for the Mg/MgH_2 thin films: the enthalpy reduction of 5kJ/mol as compared to the bulk value was calculated for the film thickness of 2 unit cell (0.16 nm Mg/ 0.30 nm MgH_2) [24]. It is not surprising, thus, that in thin films the ΔH is still very close to the value for bulk materials. Giving an example, the ΔH for hydrogen uptake by Pd capped 1 μm thick Mg thin films, as determined by resistance measurements, was similar to the value for bulk Mg [25]. The desorption enthalpy of ~ 67 kJ/mol was estimated for 600 nm -thick iron-doped Mg thin film [26]. Almost the same value of 68 kJ/mol was determined for MgH_2 formation in sandwiched Pd/Mg/Pd thin film delaminated from the substrate (to get rid of any effect related to the film clamping) [27]. The small change of ΔH in the latter two cases was probably due to the additional lattice defects introduced by doping with Fe and Pd metals.

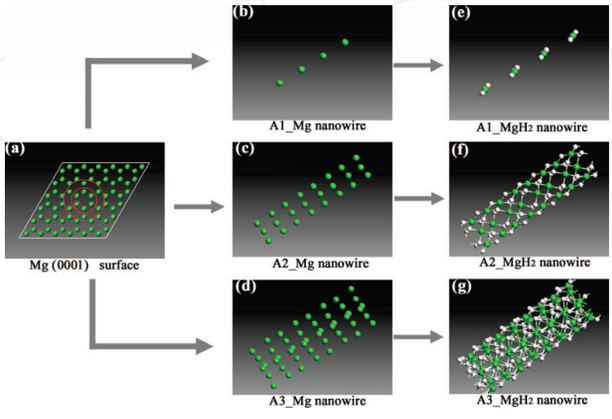


Figure 7. (a) Mg(0001) surface. Magnesium nanowires of infinite length along [0001] and the diameter size increase in the order: (b) 0.32 nm Mg nanowire; (c) 0.71 nm Mg nanowire and (d) 1.04 nm Mg nanowire. Optimized structure for (e) 0.68 nm MgH_2 nanowire; (f) 0.85 nm MgH_2 nanowire and (g) 1.24 nm MgH_2 nanowire (from Ref. [23]).

On the other hand, Baldi and coworkers showed, using hydrogenography, that it is possible to tune the thermodynamics of hydrogen absorption in Mg by means of elastic clamping [28]. They prepared the block layer 2x[Ti(10nm)/Mg(20nm)]/Pd(10nm) and proved that Pd is able to increase the hydrogen plateau pressure more than 200 times with respect to bulk Mg via the elastic constrain exerted on the expanding Mg layer. Furthermore, it was demonstrated the Mg-alloy-forming elements, such as Pd and Ni, increase substantially the hydrogen absorption plateau pressure, whereas the elements such as Ti, Nb and V, which are immiscible with Mg, are elastically disconnected from Mg and have little effect on thermodynamics properties of Mg (Figure 8). The model, based on the elastic interaction, predicted also the increase of an equilibrium hydrogen pressure with increasing Mg thickness.

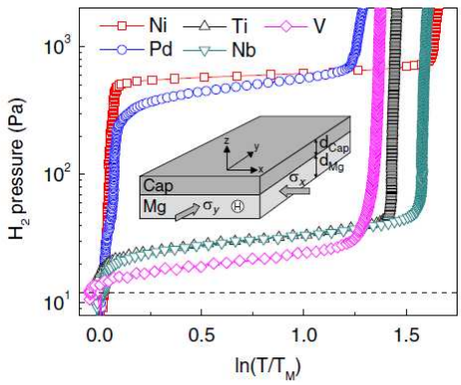


Figure 8. Effect of cap layer: PTI's measured at 333 K for Ti(10 nm)Mg(20 nm)X(10 nm)Pd(10 nm) samples deposited on glass with X = Ni, Pd, Ti, Nb, and V. The dashed line is the pressure at which coexistence of α and β phases begins to appear upon hydrogen absorption in bulk Mg. σ_x and σ_y are compressive stresses in the x and y direction due to the cap layer (from Ref. [28]).

The change in the equilibrium pressure plateaus may be also caused by clamping to the substrate which creates severe in-plane stresses in thin films during hydrogen uptake. The large impact on the thermodynamics was observed for rigid substrates which cause resistance toward volume expansion [29, 30]. The increase of p_{eq} due to the stresses caused by capping layer or a substrate would be very desirable with respect to practical application if these stresses would not relax after few hydrogen absorption/desorption cycles drawing back the p_{eq} to its original value. Moreover, the stresses relax by the formation of buckle-to-crack network, changing the structure of the thin films [31, 32]. This feature impedes the systematic studies of the interaction of the hydrogen with a metal. Recently, it was demonstrated that thin films built up on the porous, regular hexagonal AAO template, contains enough free space to allow for metals lattice unhindered expansion and, therefore, a reduction of the mechanical stress in the layer [33]. After hydrogenation, some prominent differences between two films deposited on the non-porous and porous substrate are observed (Figure 9). While in the layer deposited on the rigid glass many cracks and bulges can be observed after hydrogen absorption, the same layer deposited on the porous AAO template remains completely smooth without any cracks (compare Figure 9 (A) with (E) and (B) with (F)). In the thin film deposited on the glass locally some protrusions have appeared

as an effect of swelling of the layer (Figure 9 (C)). Based on these observations it can be concluded that a porous substrate may offer an effective way to release the stress without layer deterioration.

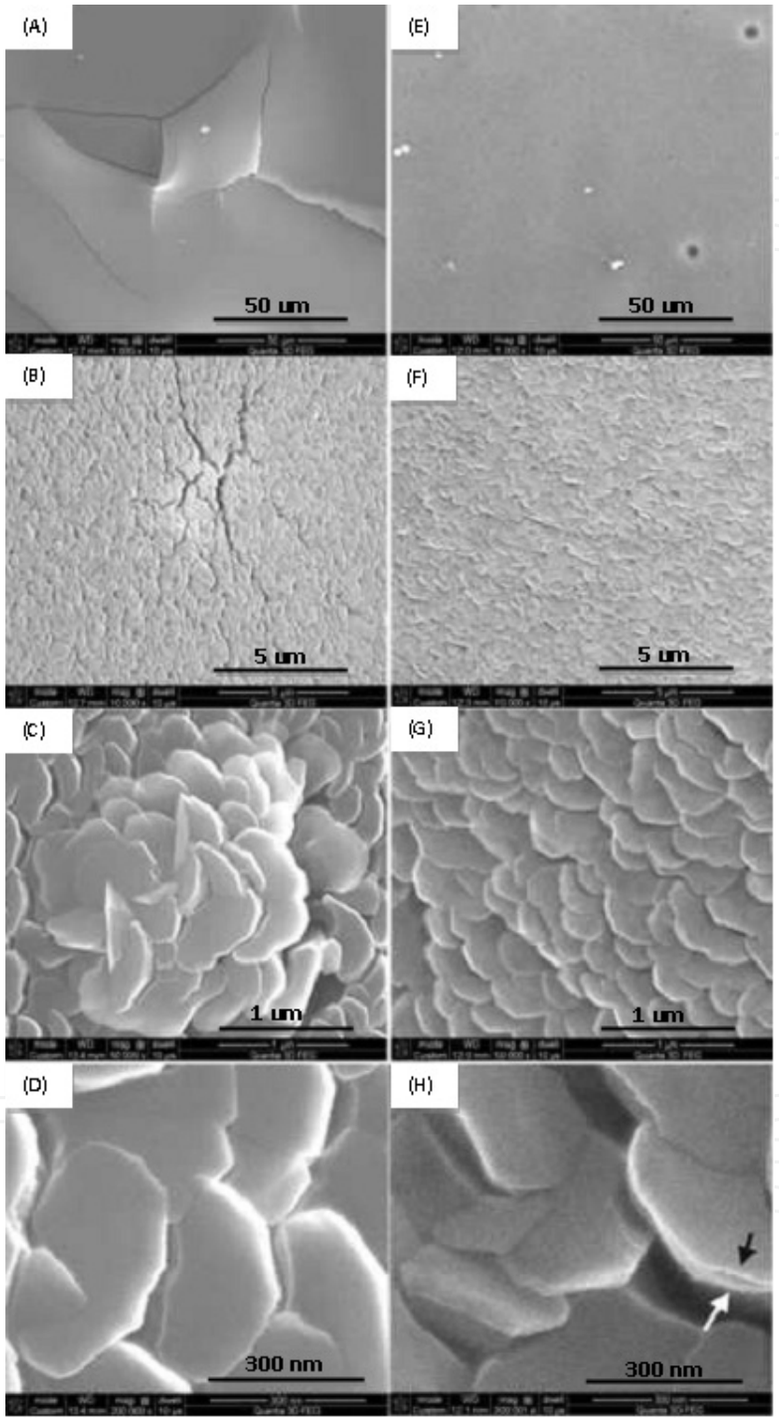


Figure 9. SEM images of Pd/Mg/Pd films on (A, B, C, D) non-porous glass substrate and (E, F, G, H) porous AAO template after hydrogenation at room temperature. Mg develops a plate-like structures of a hexagonal shape, suggesting a preferential growth along c-axis. The arrows in Figure 9(H) demonstrate that each platelet, in fact, consists of two identical hexagonal crystals stacked perfectly along their basal planes (from Ref. [33])

Another serious problem related with the hydrogenation of pure Mg is poor kinetics of process and an easiness of Mg to oxidation. The kinetics of a metal to hydride transformation is typically described by an Arrhenius type expression (Eq. 9):

$$k(T) = A\exp\left(-\frac{E_a}{k_B T}\right) \tag{9}$$

where k is the rate of the hydrogen absorption or desorption process, k_B is the Boltzmann constant, T is temperature, A the apparent pre-exponential factor and E_a – the apparent activation energy. The plot ln(k) vs. $1/k_BT$ gives, thus, the E_a value. The lower the activation energy, the faster the process. The E_a is 115-122 kJ/mol for hydrogen absorption and 126-160 kJ/mol for hydrogen desorption, as calculated for pure Mg [34]. The relation between E_a and ΔH is demonstrated graphically in Figure 10.

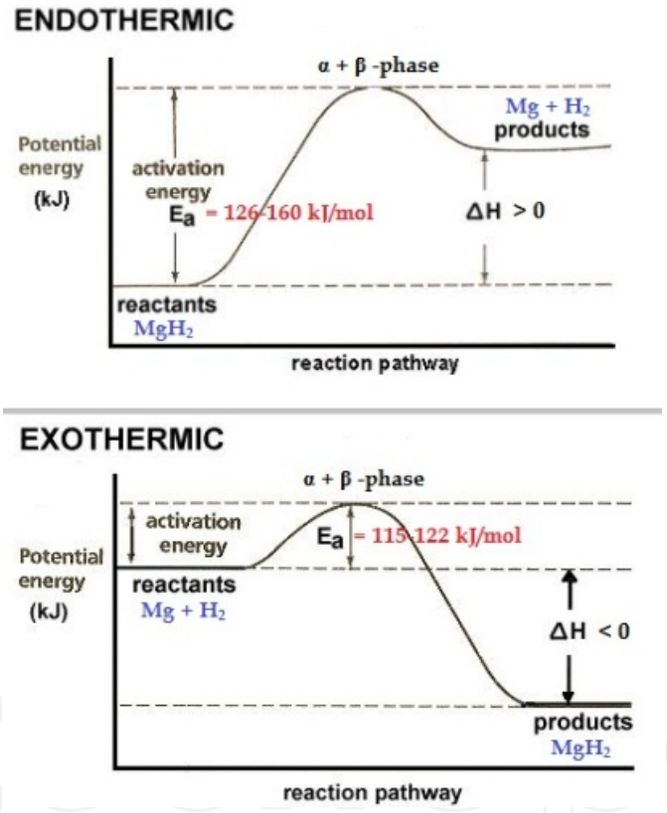


Figure 10. The relation between E_a and ΔH for Mg/MgH_2.

Reducing distances in nanoscale materials translate into faster overall reaction kinetics. Pd coating is usually applied to facilitate hydrogenation and to avoid oxidation of Mg. Hydrogen uptake for Pd-capped Mg thin films can occur at room temperature thanks to the high H_2 dissociation rate and high hydrogen diffusivity in the Pd outermost layer [35]. MgH_2 formation in thin films occurs mostly at the Pd/Mg interface where the Pd-Mg interaction is maximized. The thicker the Pd-Mg intermixing region the higher the number of Pd/Mg interfaces and the higher the hydrogen uptake can be expected [36-38]. The lattice mismatch at the interface creates defect sites with a low local electron density which

weakens the hydrogen bonding and therefore, within this interface hydrogenation of Mg occurs very fast. It was shown that the reaction at the interface control the growth of MgH_2 for the hydride layer thickness smaller than 60 nm [39]. Above the thickness hydrogenation is limited by hydrogen diffusion in the hydride layer. The overall diffusion coefficient for the Mg-to-MgH_2 transition, including nucleation and growth, was determined to be as low as $D = 1.1 \times 10^{-20}$ m^2/s [40]. Due to the extremely slow diffusion, the hydride nucleation and growth above a certain film's thickness will be practically stopped. In other words, there is a limited amount of hydrogen that can be loaded into the Mg layer above a certain thickness. It was demonstrated that the thinner Mg layer the better the hydrogen uptake rate and the higher hydrogen content at the beginning of the process. The Mg layer of 20 nm thickness has shown the best absorption kinetics with saturated hydrogen content of 5.5 wt% at 298 K and 0.7 bar H_2 [41]. The E_a for desorption process for Pd capped 100 nm thick Mg layer was determined to be 80 kJ/mol [42]. Beneficial effect of Pd was studied by hydrogenography: the rate of hydrogen absorption by Mg layer increased with Pd doping [43]. The Pd-doped Mg can absorb hydrogen at room temperature and under less than 1 bar pressure in few minutes. On the other hand, no significant influence of Pd was observed on hydrogen desorption at room temperature in air. The hydrogen release from the layer was no completed after 5h.

The enhancement of the H_2 absorption process was achieved by an electric current. The 100 nm thick Mg/Pd film, exposed to 1 bar of H_2 pressure and simultaneously to a voltage of 20-30 V, was easily hydrogenated without an external heat source [44]. Better hydriding kinetics was also observed for the films heated up to 473 K prior to hydrogenation. The annealing optimized the morphology and structure of the film in terms of finer particles size and better crystallinity [45]. No influence of the crystallization degree on absorption kinetics was, however, found by Higuchi and coworkers [46]. Yet, the crystallinity affected the hydrogen desorption kinetics which was manifested by lower desorption temperature. The lower the degree of Mg crystallization, as estimated from the intensity of Mg(002) peak in X-ray diffraction spectra, the lower the temperature at which the hydrogen was releasing. The most amorphous Mg in Pd/Mg films desorbed H_2 at a temperature lower than 463 K in vacuum of 7.0×10^{-1} Pa.

The annealing at elevated temperature can cause the alloying of Mg and Pd elements. The Mg/Pd multilayered films activated at 474 K for 2 h under 30 bar of H_2 pressure transformed completely into the Mg_6Pd phase [47]. After three cycles the films consisted of a mixture of MgPd, Mg_5Pd_2, and Mg_6Pd intermetallics phases. Qu et al. annealed the Pd/Mg film at various temperature up to 473 K in vacuum for 2 h and did not find the presence of the intermetallics [34]. It seems that in the metals interdiffusion and alloying occur dependent on whether the annealing is performed under H_2 pressure or in vacuum. To avoid the formation of the Pd-Mg intermetallics phases the tantalum (Ta) layer can be used [48]. The Ta is well-known as an excellent diffusion barrier for metals [49]. Moreover, it possesses a very high hydrogen permeability ($1{,}3 \times 10^{-7}$ mol/ms $Pa^{½}$ at 500 °C) [50].

In order to increase the Pd-Mg intermixing region, the sandwiched Pd/Mg/Pd thin films were prepared. Such systems demonstrate optimal hydrogen sorption properties not only thanks to the extended Pd/Mg interactions but also due to the cooperative phenomena. The cooperative phenomena is an elastic interaction between the two metals [51]. Upon the hydriding/dehydriding cycles both metals experience the lattice expansion/contraction. During desorption the hydrogen is first released from the Pd layers. The stress induced on the top and down surface of the Mg film, force desorption of hydrogen from Mg (Figure 11).

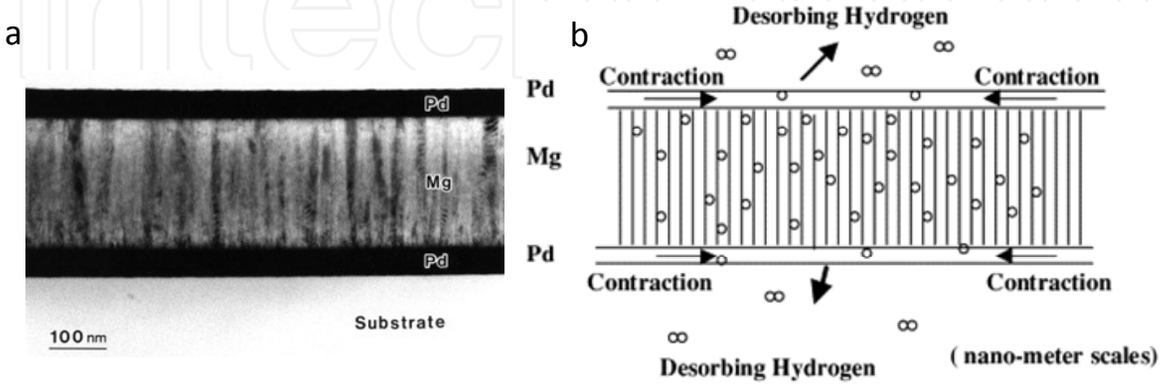


Figure 11. a) TEM micrograph for the cross section of Pd/Mg/Pd film before hydrogenation; b) scheme of hydrogenated Pd/Mg/Pd film demonstrating the cooperative effect (from Ref. [51]).

The sandwiched Pd/Mg (100 nm)/Pd thin films were fully hydrogenated at room temperature for 4h under 0.04 bar and could dehydrogenate completely and rapidly in air [52]. Hydrogen desorption process took only 20 min at 338 K, while at room temperature it lasted approximately 300 min. The overall activation energy for desorption process was estimated to be 48 kJ/mol, thus, significantly smaller than the value for pure Mg. Similar Pd/Mg/Pd films, but hydrogenated at 353K for 4h under 1 bar of H_2 pressure, exhibited the E_a of ca. 60 kJ/mol [53]. The discrepancy between the E_a values suggests that the hydrogenation conditions influence the desorption process. Faster kinetics and lower activation energy was attributed both to more extended Pd/Mg interface and to the cooperation effect.

The Mg crystallographic patterns of as-deposited Mg thin films exhibits usually strong (002) and (004) reflections implying a preferential growth along the c-axis, i.e. a single (001) out-of-plane orientation [33, 54]. MgH_2 transforms epitaxially relative to Mg according to the relation: Mg(001)//MgH_2(110) for the glass substrate and for the Al_2O_3 (001), whereas for the $LiGaO_2$ (320) substrate the relation Mg(110)//MgH_2(200) was found [55]. Due to a preferential growth along c-axis the Mg develops into a shape of hexagonal platelets (Fig. 9) forming closely packed columns (Figure 11) containing a number of polycrystalline and grain boundary defects [56, 57]. It was observed that the hydrogenation leads to a reduction of the defects. Since the defects provide the sites where hydrogen bonds are weakened and, consequently, the hydrogen migration energy is lowered leading to faster diffusion, the reduction of the defects is rather disadvantageous with respect to the hydriding/dehydriding properties. The evolution of the lattice defects in Mg during the

hydriding/dehydriding cycles was also studied by the positron annihilation spectroscopy (PAS) [58]. After the very first decomposition of MgD_2 the increase of void-like defects was observed accompanied by the decrease in deuterium storage capacity. Upon subsequent absorption and desorption cycles the concentration of these defects was reduced without, however, restoring the original storage capacity. The activation energy of desorption process decreased with the film thickness which was ascribed to a higher concentration of void-like defects in thinner layers [34].

First principle calculations show that hydrogen diffusion in MgH_2 is dominated by motions of charged defects such as positively charged vacancies at H sites, and negative H interstitials. The data are supported by some experimental observations (like for instance the enhancement of H_2 absorption by an electric current [44]). The latter type of defects dominates diffusion because the activation energy for motion of this defect is small [59]. Therefore, it should be possible to improve H diffusion by doping of Mg with charged elements which are able to increase the concentration of the diffusion defects. The DFT calculations demonstrate that only a small number of dopants have these properties [60]. In particular, the diffusion in MgH_2 can be significantly enhanced only by Co, which act as a n-type dopant that increase the concentration of negatively charged H interstitials. Nevertheless, the overall kinetics of H_2 uptake or release is also affected by lattice defects accumulated around grain boundaries and surfaces or by isolated dislocations. And the dissociation or recombination process taking place around these defects may be enhanced by other dopants.

The hydrogen sorption kinetics was significantly improved by addition of Cr-Ti bimetallic compounds [61]. At 200 °C Mg-Cr-Ti nanocomposites absorb 5 wt% hydrogen in several seconds, and desorb in 10-20 min. The influence of Ti and Fe dopants on the hydride formation was studied by infrared emission imaging of wedge-shaped thin films during hydrogen loading [62]. Ti addition did not influence Mg hydride growth rate, however, it resulted in the formation of thicker hydride layer on top of the films as compared to the un-doped Mg films. The addition of atomic fraction of 3.1% of Fe increased the hydrogenation rate by an order of magnitude and twice the MgH_2 layer thickness as compared to pure Mg. A beneficial effect of Fe on Mg hydrogenation process was thoroughly studied at temperature ranging from 363 K to 423 K by Tan et al. [26] The results suggest that Mg-Fe powders of 1-2 μm size can be fully hydrogenated within 1 min at temperature of 150 °C (423K). Catalytic effect of other transition metals was also investigated. Molybdenum plays a significant role in Mg hydrogenation [63, 64]. Mo and Ti act mainly as catalysts. The catalytic affect of NbO_x as a function of the oxygen concentration was studied [65]. The lowest activation energy for hydrogen absorption was found for the highest oxygen content (Nb_2O_5). Pure Nb does not display a considerable catalytic effect [66]. Hydrogenation kinetics was also speed up by vanadium (V) implementation into magnesium films [67]. The effect was, however, small as compared to the addition of Fe or Ti. Better effect was achieved for Mg-Cu multilayered films: Mg was fully converted to MgH_2 at temperature of 473K [68]. As will be seen in the next paragraph, a significant effect on the hydrogenation process of Mg may be exerted by the 3D transition metals which may form binary hydrides with Mg, including Co, Ni or Mn [69-71].

4. Binary and ternary Mg-based alloys

The attempts to destabilize MgH_2 (lower the desorption enthalpy) and to improve its kinetics by alloying it with transitions metals has led to discovery of many binary systems, including Mg-Ni, Mg-Fe, Mg-Co or Mg-Mn. Among these systems the magnesium – nickel hydride phases seem to be very promising candidates for hydrogen storage materials owing to a relatively high hydrogen storage capacity and low cost. The stoichiometric Mg_2Ni, due to the existence of the parent metal alloy, can be easily and reversibly hydrogenated even at room temperature. Mg_2NiH_4 has a storage capacity of 3.6 wt% and the desorption enthalpy of ~ 64 kJ/mol [72]. However, because hydrogen loading capacity increases with the Mg content, other, non-stoichiometric Mg-Ni compositions are of a special interest with respect to hydrogen storage and were intensively investigated.

An interesting hydriding properties was demonstrated for amorphous $Mg_{1.2}Ni_{1.0}$ films deposited on molybdenum [73]. It undergoes reversible hydriding/dehydriding reaction at about 150 °C and under 3.3 MPa of H_2 pressure. Moreover, based on the DSC measurement, the enthalpies for hydrogen absorption and desorption process were estimated to be -39.9 and 42.0 kJ/mole, respectively, and therefore, substantially lower than for pure Mg. The TPS (Thermal Desorption Spectroscopy) measurement for an amorphous, 1.7 nm thick, Mg_5Ni_1 thin films deposited on molybdenum, shows that hydrogen desorption starts already at 77 °C and has its maximum at around 147 °C, similarly to the $Mg_{1.2}Ni_{1.0}$ films [74]. Furthermore, the PES (Photoelectron Spectroscopy) demonstrated that no Mg segregation or desorption occurs when hydrogen is desorbed from the film, rendering the system reversible. The PCI measurement of amorphous MgNi/Pd multilayer thin films deposited on Ni substrate by magnetron sputtering revealed that up to 4.6 wt% of hydrogen can be loaded to the films at room temperature [75]. Approximately the same, reversible hydrogen content of 4.45 wt% at 224 °C has been obtained for the 1160 nm thick $Mg_{2.9}Ni$ film [76]. The $Mg_{2.9}Ni$ thin film was composed of nanocrystalline Mg_2Ni and Mg phase being of about 20-50 nm in size. The lower absorption/desorption temperature, as compared to pure Mg_2Ni and Mg systems, was attributed to the extra free energy in the interfacial region between the two nanocrystalline phases and the stress exerted on the MgH_2 phase by the adjacent Mg_2Ni, which decomposes from its hydride prior to Mg. Structural and optical properties of the Mg_yNi_{1-y} system in the composition range $0.5<y<0.95$ was studied by Gremaud and coworkers [77]. For $0.6<y<0.8$ crystalline Mg_2Ni coexists with amorphous Mg and/or Ni. After hydrogenation mostly Mg_2NiH_4 phase is present and some MgH_2 on the Mg-rich side. The abrupt structural changes is observed around the Mg-Mg_2Ni eutectic point ($y = 0.886$) which are accompanied by the drastic change in optical properties in the hydride state (Figure 12). Above the eutectic point amorphous Ni is embedded in crystalline Mg and hydrogen absorption is hampered by slow diffusion in the MgH_2 phase. Consequently a large part of Mg remains metallic. This is followed by a sudden drop in transmittance for $y > 0.886$, which one should expect to be high upon hydrogenation (Figure 12). Moreover, owing to the intimately mixed microstructure around the eutectic point, hydrogenation reaction is destabilized (the reaction occurs at lower temperature) with respect to the Mg_2Ni – Mg_2NiH_4 reaction, and

the hydrogen sorption mechanism is changed from being governed by hydrogen dissociation at the Pd capping layer to being limited by diffusion in $Mg_yNi_{1-y}H_x$ [78].

Optical properties of Pd-capped Mg_yNi_{1-y} thin films for the Mg-rich side of the Mg-Ni system ($0.7<y<0.9$) was also investigated by Yoshimura et al.[79]. The films showed much better optical transmittance upon hydrogen exposure compared to the stoichiometric Mg_2Ni compound (indicated in Figure 12 by dashed, vertical line for y = 0.667), contrary to the results obtained by Gremaud et al. which showed rather constant transmittance in the $0.7<y<0.9$ region (see Figure 12 [77]). The reason for this discrepancy may lay in the difference between the films thickness or in subtle dissimilarities between their microstructure. In agreement with the results given in Figure 12, the decrease of transmittance for Mg-poor side of the Mg-Ni system was observed by Johansson and coworkers [80]. The change in the effective optical band gap from 3.6 eV for Mg-rich to 2.4 eV for Mg-poor hydrogenated Mg-Ni alloys, was determined. Furthermore, almost linear increase of hydrogen capacity with increasing Mg content was observed.

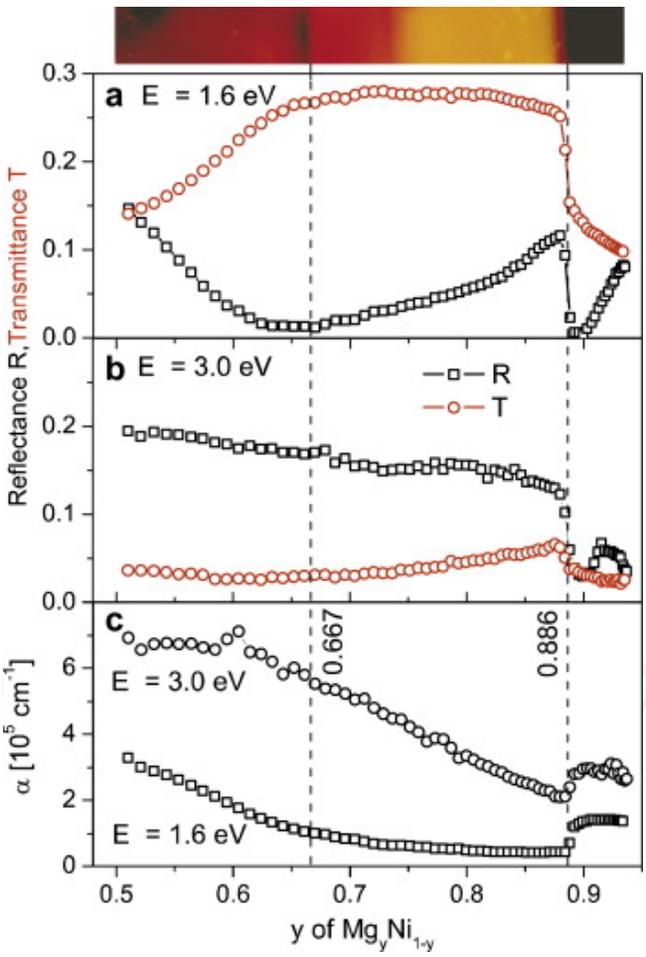


Figure 12. $Mg_yNi_{1-y}H_x$ compositional dependence of the optical reflectance (R) and transmittance (T) for two photo energies (a) $\hbar\omega$ = 1.6 eV and (b) $\hbar\omega$ = 3.0 eV. (c) Corresponding absorption coefficient α for both photon energies. At the top the optical appearance (in transmission) of a $Mg_yNi_{1-y}H_x$ gradient thin film in the hydrogenated state is shown. For y > 0.883 the film appears to be black as a result of a sudden drop in transmission (from ref. [77])

The dependence of optical properties of $Mg_yNi_{1-y}H_x$ on the alloy composition, slightly deviated from the stoichiometric Mg_2Ni, was investigated by Baldi et al. [81]. A large difference in optical behavior upon hydrogenation was explained by different hydrogen uptake mechanisms, namely, different nucleation and growth process of the hydride. Apart from a self-organized double layer structure (so-called black state): a transparent Mg_2NiH_4 layer at the substrate - film interface and a top layer of $Mg_2NiH_{0.3}$, which is always present at the beginning of hydrogenation process irrespective of the film composition, the following hydrogenation depends critically on the composition of the parent metal alloy. In slightly Mg-rich $Mg_{2\pm\delta}Ni$ films the hydrogenation proceeds by random nucleation and growth of the Mg_2NiH_4 phase within the upper metallic layer (slow process). For slightly Mg-poor $Mg_{2\pm\delta}Ni$ films hydrogenation occurs via the growth of the transparent Mg_2NiH_4 layer formed at the substrate interface (fast process). The reason for the slow hydrogenation in Mg-rich Mg_yNi_{1-y} films was explained by the presence of MgH_2, which forms prior to Mg_2NiH_4, and acts as blocking impurities for the growth of the Mg_2NiH_4 phase.

The black-state, present at a low hydrogen concentration, is characterized by low reflectance and zero transmittance in the whole visible region and suggests the application of Mg-Ni hydrides as a termochromic device for temperature control of hybrid solar collectors [82, 83]. The origin of the black state comes from preferred nucleation of Mg_2NiH_4 near the substrate/film interface after a solid solution $Mg_2NiH_{0.3}$ is formed. For achieving the black state, only a change in the first 30 nm of the films is necessary. The mixed double layer at the substrate/film interface consists of approximately 20 vol% of $Mg_2NiH_{0.3}$ and 80 vol% of Mg_2NiH_4. It was shown that the unusual hydrogen loading sequence, which starts near the substrate and not close to the catalytic Pd layer capping layer as one would expect, is due to locally enhanced kinetics [84]. Microstructural analysis revealed that up to film thickness of 50 nm, the film is built up of small grains located near the substrate, which most probably lower the activation energy, favoring nucleation of Mg_2NiH_4 [85]. The grains size increases upon further deposition, until a columnar microstructure is developed (Figure 13). After the nucleating layer is fully loaded to Mg_2NiH_4, subsequent hydrogenation process, slow or fast dependent on the composition of $Mg_{2\pm\delta}Ni$, takes place, until the entire film is loaded to semiconducting, transparent Mg_2NiH_4 (Figure 13).

The similar hydrogenation mechanism was observed for Mg-Co system [86]. Likewise the Mg-Ni, the nucleation of hydrogen rich phase (Mg_2CoH_5 in this case) initiates at the film-substrate interface. Consequently, a double layer is formed leading to the appearance of the optical black state at intermediate hydrogen concentration. In contrast, Mg-Fe showed more homogeneous hydrogen absorption. In fully loaded state in Mg-Ni and Mg-Co systems the ternary hydrides: Mg_2NiH_4 and Mg_2CoH_5, respectively, were detected, while in Mg-Fe system MgH_2 is mainly formed. The difference in hydrogen absorption mechanism is probably caused by the absence of any intermediate compound in the Mg-Fe system which does not favor the formation of Mg_2FeH_6. The presence of the black states was also observed in Mg-Mn alloys [87, 88].

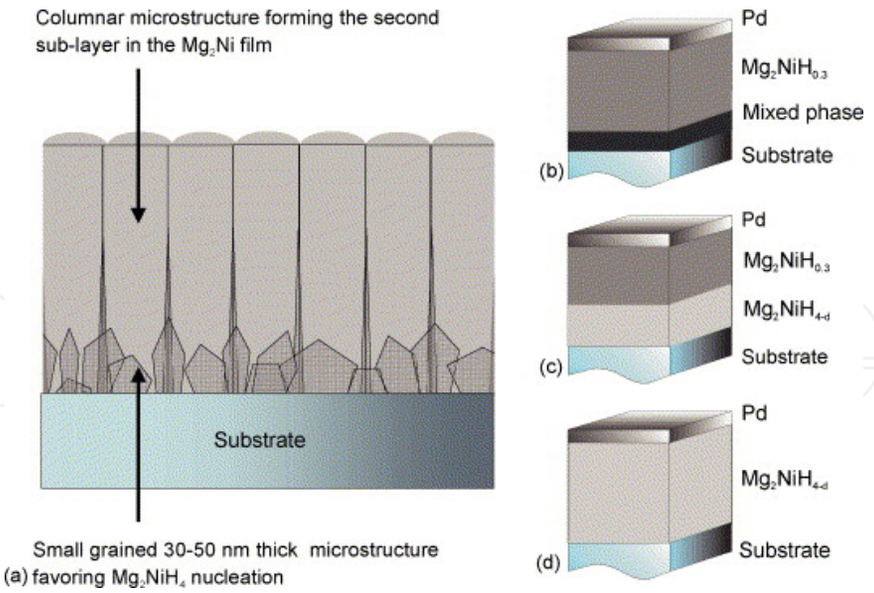


Figure 13. (a) Schematic representation of the Mg_2Ni thin film microstructure and hydrogenation mechanism for Mg-poor $Mg_{2\pm\delta}Ni$ film (fast process). The first 30–50 nm thick layer consists of small grains. From this layer, a columnar microstructure develops. At the first stage after the exposure to hydrogen a homogeneous $Mg_2NiH_{0.3}$ solid solution is formed. Nucleation of the Mg_2NiH_4 phase starts in this 30–50 nm sub-layer resulting in the optical black state (b). This layer hydrogenates to Mg_2NiH_4 and increases in thickness upon further hydrogenation resulting in a bilayer system (c). This continues until the whole film is loaded to semiconducting, transparent Mg_2NiH_4 (d) (from ref. [85]).

Mg was also alloyed with Cu to get an improved hydrogen storage properties. It was demonstrated that Pd-capped $Mg_{90}Cu_{10}$ amorphous thin film can reversibly store 5.8 wt% hydrogen in near ambient condition and could desorb it at temperature around 100 °C [89]. A comprehensive study of several metastable, crystalline single-phase $Mg_{80}X_{20}$ (X = Sc, Ti, V, Cr) thin film alloys was presented by Niessen and Notten [90]. These compounds showed high reversible hydrogen storage capacities. The best hydrogen absorption and desorption kinetics, with respect to pure Mg, was obtained in the case of Sc and Ti doping. By means of electrochemical loading $Mg_{80}Sc_{20}$ and $Mg_{80}Ti_{20}$ can reversibly store 6.7 wt% and 6.53 wt% hydrogen, respectively [91, 92]. Furthermore, it was noticed that after hydrogenation a homogeneous fcc - structured hydride is formed in both $Mg_ySc_{(1-y)}$ and $Mg_yTi_{(1-y)}$ alloys.

The structural, optical and electrical properties of the $Mg_yTi_{1-y}H_x$ thin films was thoroughly studied by Borsa et al. [93]. In metallic state all the films have zero transmission and a relatively high reflection that decreases with increasing Ti content. After hydrogen absorption under 10^5 Pa H_2 at room temperature, the reflection is low for all compositions, whereas the transmission decreases continuously with the metal ratio in the parent alloy: for $y \geq 90$ the transmission is significant, for $y < 90$ it becomes very low. Gremaued et al has presented the hydrogenography results in a form of the change of optical transmission vs $p(H_2)$ Pa for continuous gradient in the alloy composition, hydrogenated at 363K (Figure 14, ref [10]). There, a somewhat different trend was observed: the transmission is low at $p(H_2) < 10^3$ Pa but is getting higher upon decreasing y, while for the pressure approximately within

the range of $1x10^3$ Pa < $p(H_2)$ < $4x10^3$ Pa the transmission becomes high for all compositions studied (0.60 < y < 0.89).

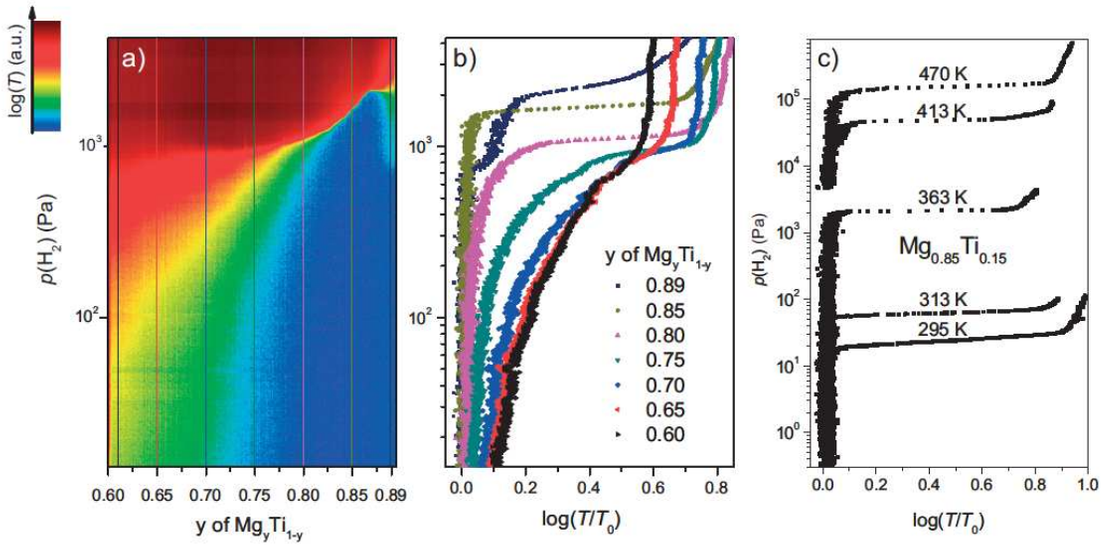


Figure 14. PTI's of Mg_yTi_{1-y} thin films with a continuous gradient in an alloy composition. a) Logarithm of the optical transmission T plotted in false colors as a function of the hydrogen pressure $p(H_2)$ and Mg atomic fraction y during hydrogenation at 363 K. Red corresponds to a high transmission and blue to a low transmission. As each column of pixels corresponds to one composition value y, the color map contains the isotherms of about 500 compositions. b) PTI's for the representative Mg–Ti alloy compositions indicated by colored vertical lines in a). c) PTI's for $Mg_{0.85}Ti_{0.15}$ at five different temperatures. The transmission T is normalized to the transmission in the metallic state T0 (from ref. [10]).

The combination of low reflection and low transmission in the hydrogenated state contributes to the highly absorbing state. Such a highly absorbing state was accounted for the presence of a mixed double layer: metallic TiH_2 and semiconducting MgH_2 phase. Based on the experimental data it was suggested that the phases do not form a composite material consisted of independent TiH_2 and MgH_2, but constitute rather a coherent structure. Hydrogenation process of the Mg_yTi_{1-y} thin films was described as follows: at very low hydrogen pressure a solid solution is formed in the Mg_yTi_{1-y} alloy, causing a small expansion of the host lattice; with increasing pressure Ti-related sites are hydrogenated at first, giving rise to the internal lattice strains release, thanks to the equality of the molar volume of TiH_2 and Mg; upon further hydrogen pressure increase, Mg is hydrogenated (Figure 15). Due to the coherent coupling between Mg and TiH_2 and the local stress induced, the Mg crystallizes to a cubic, fluorite MgH_2 structure, for y < 0.87. The complete reversibility of the system suggested that this ordering is robust and preserves upon hydrogen cycling most probably owing to the accidental equality of the molar volume of Mg and TiH_2.

Structurally, as-prepared films for all compositions have one crystalline phase that corresponds to a hexagonal Mg-Ti alloy. In the hydrogenated states the structure differs depending on the metal ratio in the parent alloy. Three regimes where identified: (1)

single fluorite phase for y < 0.87; (2) single phase rutile for y > 0.9 and (3) two phase coexistence for 0.87 < y < 0.90. The presence of a chemically partially segregated but structurally coherent metastable phase in Mg-Ti-H thin films was further confirmed by Extended X-ray Absorption Fine Structure (EXAFS) spectroscopy and by the positron Doppler broadening depth profiling method [94, 95]. Positron depth-profiling was also applied to monitor the effects of hydrogenation on thin films [96]. The analysis revealed a single homogenous layer for most metal and metal hydride films, except for the $Mg_{0.9}Ti_{0.1}H_x$ film, where a double layer was detected: a thin unloaded $Mg_{0.9}Ti_{0.1}$ or Mg-Ti-Pd alloy layer on top of a hydrogenated $Mg_{0.9}Ti_{0.1}H_x$. X-ray diffraction pattern confirmed the presence of two phases in the hydrogenated $Mg_{0.9}Ti_{0.1}$ film: one, identified as hexagonal $Mg_{0.9}Ti_{0.1}$ and a second, recognized as the rutile $Mg_{0.9}Ti_{0.1}H_2$ phase. For Ti fraction larger than about 15% only a single, broad peak in the X-ray pattern was detected, the position of which was typical for the fluorite metal hydride phase. The crystallographic analysis was confirmed by in situ recording diffraction patterns at various tilt angles, which allowed a precise identification of the crystal structures of the Mg_yTi_{1-y} thin films [97]. In the as-deposited state the film alloys have a hexagonal closed packed crystal structure. Hydrogenation under 10^5 Pa H_2 transformed the structures of $Mg_{0.7}Ti_{0.3}$ and $Mg_{0.8}Ti_{0.2}$ films into a rhombohedrally distorted unit cell with face-centered cubic (fcc) symmetry, whereas hydrogenated $Mg_{0.9}Ti_{0.1}$ has a body-centered tetragonal (bct) structure. Moreover, it was noticed that the hydrogen desorption kinetics changes along with the crystal structure from rapid for fcc-structures hydrides to sluggish for hydrides with a bct symmetry.

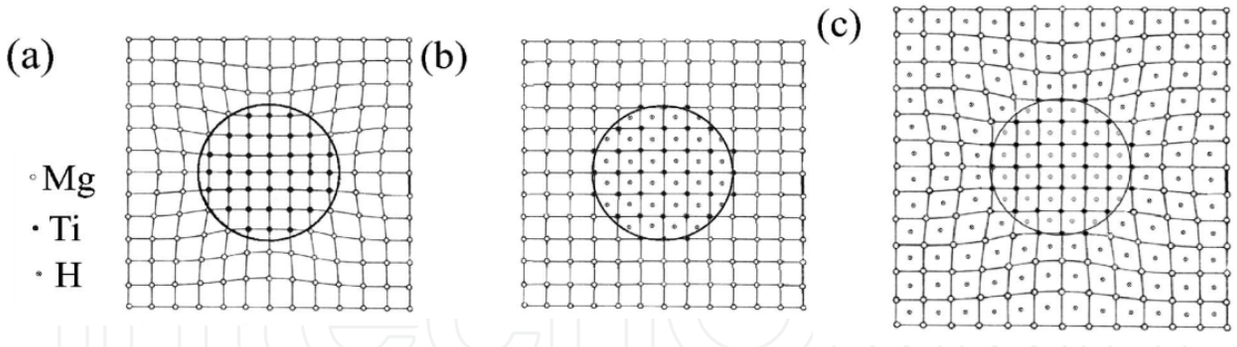


Figure 15. (a) Schematic representation of a coherent crystalline grain consisting of a Mg and Ti region. (b) The same crystalline grain after hydrogen uptake in the Ti-related sites. The accidental equality of the molar volumes of TiH_2 and Mg leads to an almost perfect crystal in situation (c). Fully hydrogenated state (from ref. [93]).

The enthalpy of hydrogenation process was established by hydrogenography [10]. For y<0.87, when the Mg-Ti hydrides have a fcc symmetry, the ΔH=-65 kJ/mol and does not differ much from the enthalpy for a bct symmetry (ΔH=-61 kJ/mol). The advantage of the fcc crystal is, however, a favorable kinetics of hydrogen diffusion within the fcc structure. The properties of the Mg-Ti thin films are very attractive for the design of hydrogen sensors, solar absorbers, or color-neutral switchable mirrors [98, 99].

The appealing kinetics of the Mg_yTi_{1-y} material has entailed the research to improve the thermodynamic of the hydrogenation process. The plateau pressure of the Mg-Ti-H system is very low (~ 0.1 Pa at room temperature). To increase the equilibrium pressure, the alloy has to be destabilized by adding additional elements. Substitution of Mg and Ti by lightweight Al or Si resulted in a shift of the plateau to higher pressures, while remaining at room temperature and maintaining a high gravimetric storage capacity of approximately 6 wt% [100]. By means of hydrogenopraphy an optimal composition in Mg-Ni-Ti system was found, $Mg_{69}Ni_{26}Ti_5$, with a relatively high hydrogen capacity (3.2 wt%) and the formation enthalpy value of -40 kJ/mol [12]. Adding Fe to the Mg-Ti system has resulted in excellent kinetics and reversible hydrogen sorption [101]. At 200 °C the Mg-Fe-Ti thin films absorbed ~ 5 wt% hydrogen in seconds and desorbed in minutes. However, rather no effect on thermodynamics of Mg-Fe-Ti was observed. The high-throughput screening technique was applied to search for an optimal material in Mg-Ti-B system [102]. The material with the composition $Mg_{0.36}Ti_{0.06}B_{0.58}$ was identified, with 10.6 wt% H_2 capacity. However, only partial reversibility was observed for the compound in the thin film.

In order to keep high hydrogen capacity of the Mg-based systems, Mg has to be destabilized with light metals, which posses a lower affinity for hydrogen. Aluminum was very often the element of choice. Beside its potential beneficial effect on kinetics and thermodynamics, the addition of Al to Mg may lead to the formation of complex hydrides, such as $Mg(AlH_4)_2$ with hydrogen storage capacities of 9.3 wt%. The magnesium alanate releases hydrogen in two steps upon heating. In the first step it desorbs 7 wt% H_2 leading to the formation of MgH_2 and Al.

Combinatorial synthesis and hydrogenation of Mg/Al libraries was prepared by electron beam physical vapor deposition at room temperature and was studied by wavelength dispersive spectroscopy (WDS) and micro-X-ray diffraction [103]. As-prepared thin films did not contain any Mg_yAl_{1-y} intermetallics or solid solution. For all Mg_yAl_{1-y} compositions full hydrogenation was obtained. MgH_2 was the main phase observed for all compositions above 20 at.% Mg. It was found that Al can act as a catalyst for hydrogenation reaction of magnesium. The hydrogenation/dehydrogenation of Pd/(Fe, Ti)/Mg-Al/(Fe, Ti)/Pd thin films was investigated [104]. The films absorb hydrogen at low temperature (~50 °C) and with excellent kinetics (few minutes). The addition of Al has improved the H_2 sorption properties and hydrogen capacities, and the catalytic effect of Ti and Fe was acknowledged.

Absorption and desorption properties of Pd-covered Mg_yAl_{1-y} alloy thin films was studied as a function of temperature and alloy composition by means of neutron reflectivity technique (NR) [105]. Hydrogen absorption was performed at 430K for 20h at 6.8 MPa. Hydrogen content and distribution in the Mg_yAl_{1-y} thin films was determined in situ. For all compositions the hydrogen was uniformly distributed throughout the MgAl film thickness (of about 52 nm for the MgAl layer and ~ 10 nm for Pd coating), whereas no hydrogen was found in the Pd layer. The $Mg_{0.7}Al_{0.3}$ film could store 4.1 wt% hydrogen with complete H_2 desorption at a temperature of 448 K. A superior absorption and desorption properties of $Mg_{0.7}Al_{0.3}$ over those of $Mg_{0.6}Al_{0.4}$ was observed. Except lower hydrogen content (3.1 wt%),

$Mg_{0.6}Al_{0.4}$ released the hydrogen at temperature around 25 K higher than $Mg_{0.7}Al_{0.3}$. Moreover, along with the higher hydrogen desorption temperature, the Pd interdiffusion into the MgAl film was noticed. A systematic study of structural change of the films during hydrogen desorption was performed later by the same group of researchers [106]. It was concluded that the Pd interdiffusion into hydrogenated MgAl film occurs for both $Mg_{0.6}Al_{0.4}$ and $Mg_{0.7}Al_{0.3}$ alloy thin films, leading to a complete destruction of the films structure. In contrast, for the as-prepared hydrogen-free Pd-coated $Mg_{0.7}Al_{0.3}$ thin film, the Pd layer remained almost intact and only small zone in the Pd/MgAl interface was infiltrated by Pd.

To prevent the interdiffusion, the Ta layer was added between the Pd and the $Mg_{0.7}Al_{0.3}$ layers (Figure 16) [107]. Tantalum was found to improve significantly hydrogen absorption kinetics due to lowering of the nucleation barrier for the formation of the hydride phase in the $Mg_{0.7}Al_{0.3}$ layer. Hydrogenation of the alloy could occur at pressure 10 time lower than for the Ta-free sample, without reducing the storage capacity. It was observed that between the catalysts (either Pd or Ta/Pd) and the $Mg_{0.7}Al_{0.3}$ layer a non-absorbing region appears, which was attributed to interfacial stress. According to the measurement ~5 wt% H can be stored in the $Mg_{0.7}Al_{0.3}$ alloy thin film under mild conditions (at room temperature and under 0.13 MPa).

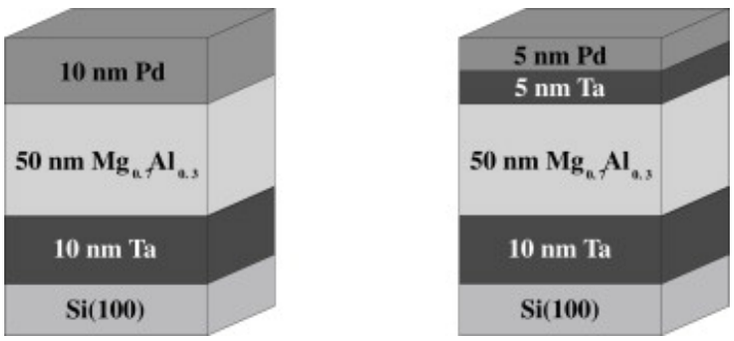


Figure 16. The structure of the film with the single Pd catalyst layer (left) and the Ta/Pd catalyst bilayer (right) (from ref. [107]).

Structure and electrochemical hydrogen storage properties of sandwiched $Pd/Mg_{1-x}Al_x/Pd$ (x=0, 0.13, 0.1, 0.39) thin films were investigated [108]. The improvement of both thermodynamics and kinetics of Mg-Al alloys as compared to pure Mg was confirmed. X-ray analysis showed that the layer was constituted of a single phase Mg(Al) solid solution. All films demonstrates a globular surface structure (Figure 17). The surface roughness of the films depends on the Al concentration. In the absence of Al (x=0) the surface was very rough and consisted of large particles. Upon the Al increase the surface was becoming smoother. Also porosity depends on the Al concentration. The best hydriding properties was detected for the $Pd/Mg_{0.79}Al_{0.21}/Pd$ thin films (storage capacity of ~ 1.9 wt%), which was related to a high porosity of the film (28%).

The complex $Mg(AlH_4)_2$ hydride was experimentally observed by Jain et al. [109]. A sandwiched-like Pd/Al/Mg/Pd thin film was hydrogenated at 150 °C under 0.2 MPa H_2 pressure for 2h. The formation of the $Mg(AlH_4)_2$ along with MgH_2, formed mostly at the

Pd/Mg interface, has eliminated the generation of Mg_xPd_y intermetallics and reduced the oxygen content in the film. Moreover, an increment in hydrogen storage capacity was noticed. The $Mg(AlH_4)_2$ was also obtained under high-flux, low-energy hydrogen ion irradiation of Mg/Al bilayer films [110, 111]. Its synthesis takes place under intensive intermixing of Mg and Al atoms and with continuous supply of hydrogen. The 2 keV hydrogen ions pass the naturally formed 2 – 4 nm thick Al_2O_3 layer without destroying it. Moreover, it was suggested that the magnesium alanate was protected by the Al_2O_3 layer. The experimental results have confirmed a two-step decomposition mechanism of the $Mg(AlH_4)_2$ and demonstrated that dehydrogenation is controlled by transport process through the oxide layer.

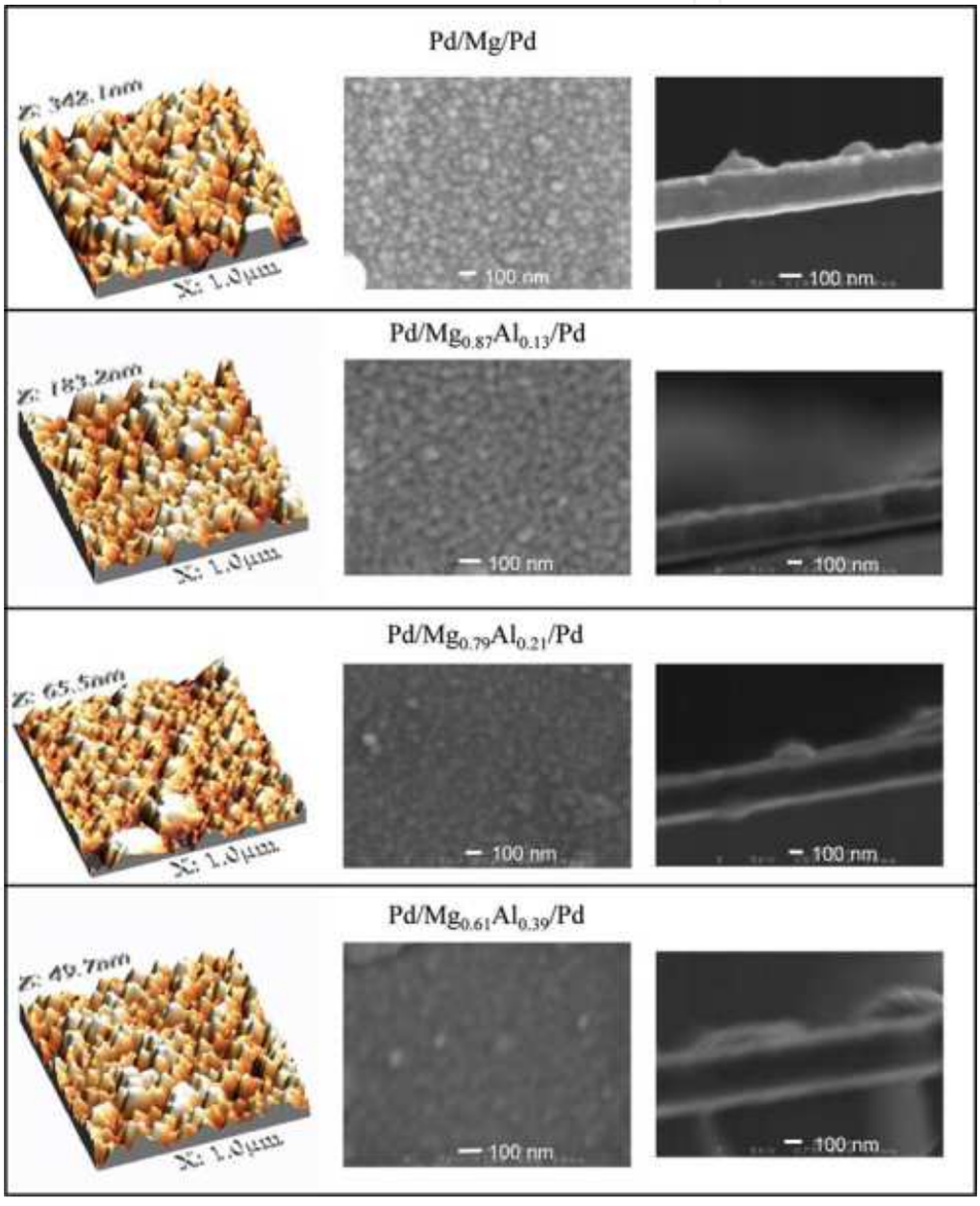


Figure 17. 3D AFM images, surface and cross-section SEM images of the $Pd/Mg_{1-x}Al_x/Pd$ films with x = 0, 0.13, 0.21 and 0.39 from top to bottom (from ref. [108]).

5. Conclusion

Notwithstanding the remarkable achievements in hydrogen absorption–desorption attained for thin films, it remains difficult to transfer the results to bulk materials (powders), which are thought to be used in transport sector. The difficulties originates from the fact that the hydrogen interaction with mater depends strongly on a subtle tuning between parameters such as: a number and type of defects, microstructure, size and morphology of crystallites, which are not easy controllable by the application of the powders preparation methods, like for instance mechanical milling, as compared to the thin films deposition techniques. As an example, mechanically milled Mg-Ti powders display much slower kinetics, reduced storage capacities and lower structural stability as compare to the Mg-Ti thin films [112]. The thin films synthesis methods can lead to the formation of non-equilibrium phases, which are rather not accessible by bulk preparation methods. In contrast to bulk preparation techniques, in a thin film approach it is relatively easy to control the size and morphology of material. The size reduction to the nanoscale leads to the energy contributions which are typically negligible in bulk, including the interaction of the sample with the substrate, surface or interface energies and quantum size effects. These contributions allows one to overcome the hydrogenation kinetics limitations and to study the intrinsic thermodynamic properties of hydrogen absorption. Thin films are particularly suited for combinatorial techniques: allowing one to perform combinatorial research on thousands of different concentrations of elements at once. It helps to identify an optimal alloy's composition and to find the best catalyst for hydrogen sorption. Moreover, other technological applications for thin films, such as in batteries, coatings, or solar collectors, have been proposed due to discovered spectacular changes in the optical properties of metal–hydride films near their metal–insulator transition ("switchable mirror" behavior). The transition is reversible and can be simply induced by changing the surrounding hydrogen gas pressure or electrolytic cell potential.

Author details

Małgorzata Norek
Department of Advanced Materials and Technology, Military University of Technology, Warsaw, Poland

Acknowledgement

Thanks are due to Prof. Leszek R. Jaroszewicz from Military University of Technology in Warsaw, Poland, and to the Polish Ministry of Science and Higher Education, Key Project POIG.01.03.01-14-016/08 for the financial support.

6. References

[1] Remhof A, Borgschulte A (2008) Thin-Film Metal Hydrides. ChemPhysChem 9: 2440-2455.

[2] Cuevas F, Joubert J-M, Latroche M, Percheron-Guegan A Intermetallic compounds as negative electrodes of Ni/MHbatteries (2001) Appl. Phys. A 72: 225-238.
[3] More information can be found at the website: http://www.ncnr.nist.gov/programs/reflect/
[4] Remhof A, Song G, Sutter Ch, Schreyer A, Siebrecht R, Zabel H (1999) Hydrogen and deuterium in epitaxial Y (0001) films: Structural properties and isotope exchange. Phys. Rev. B 59: 6689.
[5] Ingason A S, Olafsson S (2005) Thermodynamics of hydrogen uptake in Mg films studied by resistance measurements. J. Alloys and Compd. 404-406: 469-472.
[6] Demènech-Ferrer R, Rodrìguez-Viejo J, González-Silveira, Garcia G (2011) In situ infrared thermographic screening of compositional spread Mg-Ti. J. Alloys and Compd. 509: 6497-6501.
[7] Olk CH, Tibbetts GG, Simon D, Moleski JJ (2003) Combinatorial preparation and infrared screening of hydrogen sorbing metal alloys. J. Appl. Phys 94: 720.
[8] Olk CH (2005) Combinatorial approach to material synthesis and screening of hydrogen storage alloys. Meas. Sci. Technol. 16: 14-20.
[9] Oguchi H, Tan Z, Heilweil EJ, Bendersky LA (2010) In-situ infrared imaging methodology for measuring heterogeneous growth process of a hydride phase. Int. J. Hydrogen Energy 35: 1296-1299.
[10] Gremaud R, Broedersz CP, Borsa DM, Borgschulte A, Mauron P, Screuders H, Rector JH, Dam B, Griessen R (2007) Hydrogenography: an optical combinatorial method to find new light-weight hydrogen-storage materials. Adv. Mater. 19: 2813-2817.
[11] Borgschulte A, Lohstroh W, Westerwaal RJ, Schreuders H, Rector JH, Dam B, Griessen R (2005) Combinatorial method for the development of a catalyst promoting hydrogen uptake. J. Alloys and Compd. 404-406: 699-705.
[12] Dam B, Gremaud R, Broedersz C, Griessen R (2007) Combinatorial thin films methods for the search of new lightweight metal hydrides. Scripta Mater. 56: 853-858.
[13] Gremaud R, Slaman M, Schreuders H, Dam B, Griessen R (2007) An optical method to determine the thermodynamics of hydrogen absorption and desorption in metals. Appl. Phys. Lett. 91: 231916.
[14] Ludwig A, Cao J, Savan A, Ehmann M (2007) Hugh-throughput characterization of hydrogen storage materials using thin films on macromachined Si substrates. J. Alloys and Compd. 446-447: 516-521.
[15] Ludwig A, Cao J, Dam, B, Gremaud R (2007) Opto-mechanical characterization of hydrogen storage properties of Mg-Ni thin film composition spreads. Appl. Surf, Sci. 254: 682-686.
[16] Woo NC, Ng BG, van Dover RB (2007) High-throughput combinatorial study of local stress in thin films composition spreads. Rev. Sci. Instrum. 78: 072208.
[17] Guerin S, Hayden BE, Smith DCA (2008) High-throughput synthesis and screening of hydrogen – storage alloys. J. Comb. Chem. 10: 37-43.
[18] Züttel A (2003) Materials for hydrogen storage. Materials Today 6: 24–33.
[19] Krozer A, Kasemo B (1987) Unusual kinetics due to interface hydride formation in the hydriding of Pd/Mg sandwich layers. J Vac Sci Technol A 5: 1003-1005.

[20] Pozzo M, D. Alfè D (2008) Structural properties and enthalpy of formation of magnesium hydride from quantum Monte Carlo calculations. Phys. Rev. B 77: 104103.
[21] Aguey-Zinsou KF, Ares-Fernandez JR (2008) Synthesis of Colloidal Magnesium: A Near Room Temperature Store for Hydrogen. Chem. Mater. 20: 376-378.
[22] Cheung S, Deng WQ, van Duin ACT, Goddard III WA (2005) ReaxFFMgH Reactive Force Field for Magnesium Hydride Systems. J. Phys. Chem. A 109: 851-859.
[23] Li L, Peng B, Ji W, Chen J (2009) Studies on the Hydrogen Storage of Magnesium Nanowires by Density Functional Theory. J. Am. Chem. Soc. 113, 3007–3013
[24] Liang JJ (2005) Theoretical insight in tailoring energetic of Mg hydrogen absorption/desorpion through nano-engineering. Appl. Phys. A 80: 173-178.
[25] Ingason AS, Olafsson S (2005) Thermodynamics of hydrogen uptake in Mg films studied by resistance measurements. J Alloys Compd 404-406: 469-472.
[26] Tan Z, Chiu C, Heilweil EJ, Bendersky LA (2011) Thermodynamics, kinetics and microstructural evolution Turing hydrogenation of iron-doped magnesium thin films. Int. J. Hydrogen Energy 36: 9702-9713.
[27] Barcelo S, Rogers M, Grigoropoulos CP, Mao SS (2010) Hydrogen storage property of sandwiched magnesium hydride nanoparticle thin film." International Journal of Hydrogen Energy 35: 7232 – 7235.
[28] Baldi A, Gonzalez-Silveira M, Palmisano V, Dam B, Griessen R (2009) Destabilization of the Mg-H system through elastic constrains. Phys. Rev. Lett. 102: 226102.
[29] Nicolas M, Dumoulin L, Burger JP (1986) Thickness dependence of the critical solution temperature of hydrogen in Pd films. J. Apl. Phys. 60: 3125.
[30] Vermeulen P, Ledovskikh A, Danilov D, Notten HL (2006) The impact of the layer thickness on the thermodynamics properties of Pd hydride thin film electrodes. J. Phys. Chem. B 110: 20350-20353.
[31] Siviero G, Bello V, Mattei G, Mazzoldi P, Battaglin G, Bazzanella N, Checchetto R, Miotello A (2009) Structural evolution of Pd-capped Mg thin films under H2 absorption and desorption cycles. Int J Hydrogen Energy 34: 4817-4826.
[32] Gremaud R, Gonzalez-Silveira M, Pivak Y, de Man S, Slaman M, Schreuders H, Dam B, Griessen R (2009) Hydrogenography of PdHx thin films: Influence of H-induced stress relaxation processes. Acta Materialia 57: 1209-1219.
[33] Norek M, Stępniowski WJ, Polański M, Zasada D, Bojar Z, Bystrzycki J (2011) A comparative study on the hydrogen absorption of thin films at room temperature deposited on non-porous glass substrate and nano-porous anodic aluminum oxide (AAO) template. Inter. J. Hydrogen Energy 36: 11777-11784.
[34] Norberg NS, Arthur TS, Fredrick SJ, Prieto AL (2011) Size-Dependent Hydrogen Storage Properties of Mg Nanocrystals Prepared from Solution. J. Am. Chem. Soc. 133: 10679–10681.
[35] Yoshimura K, Yamada Y, Okada M (2004) Hydrogenation of Pd capped Mg thin films at room temperature. Surf Sci 566-568: 751-754.
[36] Paillier J, Bouhtiyya S, Ross GG, Roué L (2006) Influence of the deposition atmosphere on the Pd/Mg interface characteristics of hydriding Pd-Mg thin films prepared by pulsed laser deposition. Thin Solid Films 500: 117-123.

[37] Zhdanov VP, Krozer A, Kasemo B (1993) Kinetics of first-order phase transitions initiated by diffusion of particles from the surface into the bulk. Phys Rev B 47: 11044-11048

[38] Paillier J, Roue (2005) Hydrogen electrosortpion and structural properties of nanostructured Pd/Mg thin films elaborated by pulse laser deposition. J. Alloys Compd 404-406: 473-476.

[39] Kelly ST, Clemens BM (2010) Moving interface hydride formation in multilayered metal thin films. J. Appl. Phys. 108: 013521.

[40] Spatz P, Aebischer HA, Krozer A, Schlapbach L (1993) The Diffusion of H in Mg and the Nucleation and Growth of MgH2 in Thin Films. Z. Phys. Chem. 181: 393-397

[41] Qu J, Sun B, Yang R, Zhao W, Wang Y, Li X. (2010) Hydrogen absorption kinetics of Mg thin films under mild conditions. Script. Mater. 62: 317-320.

[42] Qu J, Wang Y, Xie L, Zheng J, Liu Y, Li X, (2009) Superior hydrogen absorption and desorption behavior of Mg thin films. J Power Sources 186: 515-520.

[43] Pasturel M, Slaman M, Schreuders H, Rector JH, Borsa DM, Dam B, Griessen R (2006) Hydrogen absorption kinetics and optical properties of Pd-doped Mg thin films. J. Appl. Phys 100: 023515.

[44] Borgschulte A, Rector JH, Schreuders H, Dam B, Griesssen R (2007) Electrohydrogenation of MgH2-thin films. Appl. Phys. Lett. 90: 071912.

[45] Qu J, Wang Y, Xie L, Zheng J, Liu Y, Li X (2009) Hydrogen absorption–desorption, optical transmission properties and annealing effect of Mg thin films prepared by magnetron sputtering. Int J Hydrogen Energy 34: 1910-1915.

[46] Higuchi K, Kajioka H, Toiyama K, Fujii H, Orimo S, Kikuchi Y (1999) In situ study of hydriding–dehydriding properties in some Pd/Mg thin films with different degree of Mg crystallization. J Alloys Compd 293-295: 484-489.

[47] Ye SY, Chan SLI, Ouyang LZ, Zhu M (2010) Hydrogen storage and structure variation in Mg/Pd multi-layer film. J Alloys Compd 504: 493-497.

[48] Tan X, Harrower CT, Amirkhiz BS, Mitlin D (2009) Nano-scale bi-layer Pd/Ta, Pd/Nb, Pd/Ti and Pd/Fe catalysts for hydrogen sorption in magnesium thin films. Int. J. Hydrogen Energy 34: 7741-7748.

[49] Hoogeveen R, Moske M, Geisler H, Samwer K (1996) Texture and phase transformation of sputter-deposited metastable Ta films and Ta/Cu multilayers. Thin Solid Films 275: 203-206.

[50] Ockwig NW, Nenoff TM (2007) Membranes for hydrogen separation. Chem Rev. 107: 4078-4110.

[51] Higuchi K, Yamamoto K, Kajioka H, Toiyama K, Honda M, Orimo S, Fujii H (2002) Remarkable hydrogen storage properties in three-layered Pd/Mg/Pd thin films. J Alloys Compd 330-332: 526-530.

[52] Qu J, Sun B, Zheng J, Yang R, Wang Y, Li X (2010) Hydrogen desorption properties of Mg thin films at room temperature. J. Power Sources 195: 1190-1194.

[53] Qu J, Sun B, Liu Y, Yang R, Li Y, Li X (2010) Improved hydrogen storage properties in Mg-based thin films by tailoring structures. Int J Hydrogen Energy 35: 8331 – 8336.

[54] [54]Özgit Ç, Akyıldız H, Öztürk T (2010) Isochronal hydrogenation of textured Mg/Pd thin films Thin Solid Films 518: 4762 – 4767

[55] Kelekar R, Giffard H, Kelly ST, Clemens BM (2007) Formation and dissociation of MgH2 in epitaxial Mg thin films. J. Appl. Phys. 101: 114311.

[56] Singh S, S. Eijt WH, Zandbergen MW, Legerstee WJ, Svetchnikov VL, (2007) Nanoscale structure and the hydrogenation of Pd-capped magnesium thin films prepared by plasma sputter and pulsed laser deposition. J. Alloys Compd. 441: 344-351.

[57] Yamamoto K, Higuchi K, Kajioka H, Sumida H, Orimo S, Fujii H (2002) Optical transmission of magnesium hydride thin film with characteristic nanostructure. J Alloys Compd 330-332: 352-356.

[58] Checchetto R, Bazzanella N, Miotello A, Brusa R, Zecca A, Mengucci A (2004) Deuterium storage in nanocrystalline magnesium thin films. J. Appl. Phys. 95: 1989-1995.

[59] Hao S, Sholl DS (2008) Hydrogen diffusion in MgH2 and NaMgH3 via concerted motions of charged defects. Appl. Phys. Lett. 93: 251901.

[60] Hao S, Sholl DS (2009) Selection of dopants to enhance hydrogen diffusion rates in MgH2 and NaMgH3. Appl. Phys. Lett. 94: 171909.

[61] Zahiri B, Amirkhiz BS, Mitlin D (2010) Hydrogen storage cycling of MgH2 thin film nanocomposites catalyzed by bimetallic Cr Ti. Appl. Phys. Lett. 97: 083106.

[62] Tan Z, Heilweil EJ, Bendersky LA (2010) In-situ kinetics studies on hydrogenation of transition metal (=Ti, Fe) doped Mg films. Mater. Res. Soc. Symp. Proc. 1216: 148-152.

[63] Stolz SE, Popovic D (2007) A high-resolution core-level study of Ni-catalyzed absorption and desorption of hydrogen in Mg-films. Surf. Sci. 601:1507-1512.

[64] Farangis B, Nachimuthu P, Richardson TJ, Slack JL, Meyer BK, Perera RCC, Rubin MD (2003) Structural and electronic properties of magnesium-3D transition metal switchable mirrors. Solid State Ionics 165: 309-314.

[65] Borgschulte A, Lohstroh W, Westerwaal RJ, Schreuders H, Rector JH, Dam B, Griessen R (2005) Combinatorial method for the development of a catalyst promoting hydrogen uptake. J. Alloys and Compd. 404-406: 699-705.

[66] Mosaner P, Bazzanella N, Bonelli M, Checcetto R, Miotello A (2004) Mg: Nb films produced by pulsed laser deposition for hydrogen storage. Mater. Sci. Eng. B 108: 33-37.

[67] Leon A, Knystautas EJ, Huot J, Russo SL, Koch CH, Schulz R (2003) Hydrogen sorption properties of vanadium- and palladium-implanted magnesium films. J. Alloys and Compd. 356-357: 530-535.

[68] Akyıldız H, Özenbas M, Öztürk T (2006) Hydrogen absorption in magnesium based crystalline thin films. Int. J. Hydrogen Energy 31: 1379-1383.

[69] Richardson TJ, Farangis B, Slack JL, Nachimuthu P, Perera R, Tamura N, Rubin M (2003) X-ray absorption spectroscopy of transition metal-magnesium hydride thin films. J. Alloys and Compd. 356-357: 204-207.

[70] Farangis B, Nachimuthu P, Richardson TJ, Slack JL, Perera R, Gullikson EM, Lindle DW, Rubin M (2003) In situ x-ray-absorption spectroscopy study of hydrogen absorption by nickel-magnesium thin films. Phys. Rev. B 67: 085106.

[71] Richardson TJ, Slack JL, Farangis B, Rubin MD (2002) Mixed metal films with switchable optical properties. Appl. Phys. Lett. 80: 1349-1351.
[72] Reilly JJ, Wiswall RH (1968) Reaction of hydrogen with alloys of magnesium and nickel and the formation of Mg2NiH4. Inorg. Chem. 7: 2254-2256.
[73] Chen J, Yang H-B, Xia Y-Y, Kuriyama N, Xu Q, Sakai T (2002) Hydriding and dehydriding properties of amorphous magnesium-nickel films prepared by a sputtering method. Chem Mater. 14: 2834-2836.
[74] Stoltz SE, Stoltz D (2007) Spectroscopic evidence for reversible hydrogen storage in unordered Mg5Ni1 thin films. J. Phys.: Condens. Matter 19: 446010.
[75] Ouyang LZ, Wag H, Chung CY, Ahn JH, Zhu M (2006) MgNi/Pd multilayer hydrogen storage thin films prepared by dc magnetron sputtering. J. Alloys and Compd. 422: 58-61.
[76] Quyng LZ, Ye SY, Dong HW, Zhu M (2007) Effect of interfacial free energy on hydriding reaction of Mg-Ni thin films. Appl. Phys. Lett. 90: 021917.
[77] Gremaud R, van Mechelen JLM, Schreuders H, Slaman M, Dam B, Griessen R (2009) Structural and optical properties of MgyNi1-yHx gradient thin films in relation to the as-deposited metallic state. Int. J. Hydrogen Energy 34: 8951-8957.
[78] Gremaud R, Broedersz CP, Borgschulte A, van Setten MJ,, Schreuders H, Slaman M, Dam B, Griessen R (2010) Hydrogenography of MgyNi1-yHx gradient thin films: interplay between the thermodynamics ad kinetic of hydrogenation. Acta Mater. 58: 658-668.
[79] Yoshimura K, Yamada Y, Okada M (2002) Optical switching of Mg-rich Mg-Ni alloy thin films. Appl. Phys. Lett. 81: 4709-4711.
[80] Johansson E, Chacon C, Zlotea C, Andersson Y, Hjorvarsson B (2004) Hydrogen uptake and optical properties of sputtered Mg-Ni thin films. J. Phys.: Condens. Matter 16: 7649-7662.
[81] Borsa DM, Lohstroh W, Gremaud R, Rector JH, Dam B, Wijngaarden RJ, Griessen R (2007) Critical composition dependence of the hydrogenation of Mg2±δNi thin films. J. Alloys and Compd 428: 34-39.
[82] Lokhorst AC, Dam B, Giebels IAME, Welling MS, Lohstroh W, Griessen R (2005) Thermochromic metal-hydride bilayer devices. J. Alloys and Compd. 404-406: 465-468.
[83] Mechelen JLM, Noheda B, Lohstroh W, Westerwaal RJ, Rector JH, Dam B, Griessen R (2004) Mg-Ni-H films as selective coatings: Tunable reflectance by layered hydrogenation. Appl. Phys. Lett. 84: 3651-3653.
[84] Lohstroh W, Westerwaal RJ, Mechelen JLM, Chacon C, Johanssson E, Dam B, Griessen R (2004) Structural and optical properties of Mg2NiHx switchable mirrors upon hydrogen loading. Phys. Rev. B 70: 165411.
[85] Westerwaal RJ, Borgschulte A, Lohstroh W, Dam B, Kooi B, Brink G, Hopstaken MJP, Notten PHL (2006) The growth-induced microstructural origin of the optical black states of Mg2NiHx thin films. J. Alloys and Compd. 416: 2-10.
[86] Lohstroh W, Westerwaal RJ, Lokhorst AC, Mechelen JLM, Dam B, Griessen R (2005) Double layer formation in Mg-TM switchable mirrors (TM: Ni, Co, Fe). J. Alloys and Compd. 404-406: 490-493.

[87] Richardson TJ, Slack JL, Farangis B, Rubin MD (2002) Mixed metal films with switchable optical properties. Appl. Phys. Lett. 80: 1349-1351.

[88] Jangid MK, Singh M (2012) Hydrogenation and annealing effect on electrical properties of nanostructured Mg/Mn bilayer thin films. Int. J. Hydrogen Energy 37: 3786-3791.

[89] Akyıldız H, Öztürk T (2010) Hydrogen sorption in crystalline and amorphous Mg-Cu thin films. J. Alloys and Compd. 492: 745-750

[90] Niessen RAH, Notten PHL (2005) Electrochemical Hydrogen Storage Characteristics of Thin Film MgX (X=Sc, Ti, V, Cr) Compounds. Electrochem. Solid-State Lett. 8: A534-A538.

[91] Niessen RAH, Notten PHL (2005) Hydrogen storage in thin film magnesium-scandium alloys. J. Alloys and Compd. 404-406: 457-460.

[92] Vermeulen P, Niessen RAH, Notten PHL (2006) Hydrogen storage in metastable MgyTi(1-y) thin films. Electrochem. Comm. 8: 27-32.

[93] Borsa DM, Gremaud R, Baldi A, Schreuders H, Rector JH, Kooi B, Vermeulen P, Notten PHL, Dam B, Griessen R (2007) Structural, optical, and electronical properties of MgyTi1-yHx thin films. Phys. Rev. B 75: 205408.

[94] Baldi A, Gremaud R, Borsa DM, Balde CP, Eerden AMJ, Kruijzer GL, Jongh PE, Dam B, Griessen R (2009) Nanoscale composition modulations in MgyTi1-yHx thin films alloys for hydrogen storage. Int. J. Hydrogen Energy 34: 140-1457.

[95] Leegwater H, Schut H, Egger W, Baldi A, Dam B, Eijt SWH (2010) Divacancies and the hydrogenation of Mg-Ti films with short range chemical order. Appl. Phys. Lett. 96: 151902.

[96] Eijt SWH, Leegwater H, Schut H, Anastasopol A, Egger W, Ravelli L, Hugenschmidt C, Dam B (2011) Layer-resolved study of the Mg to MgH2 transformation in Mg-Ti films with short-range chemical order. J. Alloys and Compd. 509S: S567-S571.

[97] Vermeulen P, Graat PCJ, Wondergem HJ, Notten PHL (2008) Crystal structures of MgyTi100-y thin film alloys in the as-deposited and hydrogenated state. Int. J. Hydrogen Energy 33: 5646-5650.

[98] Slaman M, Dam B, Pasturel M, Borsa DM, Schreuders H, Rector JH, Griessen R Fiber optic hydrogen detectors containing Mg-based metal hydrides. Sensor Actuat. B Chem. 123: 538-545.

[99] Bao S, Tajima K, Yamada Y, Okada M, Yoshimura K (2007) Color-neutral switchable mirrors based on magnesium-titanium thin films. Appl. Phys. A 87: 621-624.

[100] Vermeulen P, Thiel EFMJ, Notten PHL (2007) Ternary MgTiX-alloys: a promising route towards low-temperature high-capacity, hydrogen storage materials. Chem. Eur. J. 13: 9892-9898.

[101] Zahiri B, Harrower CT, Amirkhiz BS, Mitlin D (2009) Rapid and reversible hydrogen sorption in Mg-Fe-Ti thin films. Appl. Phys. Lett. 95: 103114.

[102] Amieiro-Fonseca A, Ellis SR, Nuttall JC, Hayden BE, Guerin S, Purdy G, Soulie JP, Callear SK, Culligan SD, David WIF, Edwards PP, Jones MO, Johnson SR, Pohl AH (2011) A multidisciplinary combinatorial approach for tuning promising hydrogen storage materials towards automotive applications. Faraday Discuss. 151: 369-384.

[103] Garcia G, Domenech - Ferrer R, Pi F, Santiso J, Rodriguez-Viejo J (2007) Combinatorial synthesis and hydrogenation of Mg/Al libraries prepared by electron beam physical vapor deposition. J. Comb. Chem. 9: 230-236.

[104] Domenech - Ferrer R, Sridharan MG, Garcia G, Pi F, Rodriguez-Viejo J (2007) Hydrogen properties of pure magnesium and magnesium-aluminium thin films. J. Power Sources 169: 117-122.

[105] Fritzsche H, Saoudi M, Haagsma J, Ophus C, Luber C, Harrower CT, Mitlin (2008) Neutron reflectometry study of hydrogen desorption in destabilized MgAl alloy thin films. Appl. Phys. Lett. 92: 121917.

[106] Fritzsche H, Saoudi M, Haagsma J, Ophus C, Luber C, Harrower CT, Mitlin (2009) Structural changes of thin MgAl films during hydrogen desorption. Nucl. Instr. And Meth. A 600: 301-304.

[107] Harrower C, Poirier E, Fritzsche H, Kalisvaart P, Satija S, Akgun B, Mitlin D (2010) Early deuteration steps of Pd- and Ta/Pd-catalyzed Mg70Al30 thin films observed at room temperature. Int. J. Hydrogen energy 35: 10343-10348.

[108] Bouhtiyya S, Roue L (2010) Structure and electrochemical hydrogen storage properties of Pd/Mg1-x Alx/Pd thin films prepared by pulsed laser deposition. J. Mater. Sci. 45: 946-952.

[109] Jain P, Jain A, Vyas D, Kabiraj D, Khan SA, Jain IP (2012) Comparative study on hydrogenation properties of Pd capped Md and Mg/Al. films. Int. J. Hydrogen Energy 37: 3779-3785.

[110] Pranevicius LL, Milcius D (2005) Synthesis of Mg(AlH4)2 in bilayer Mg/Al thin films under plasma immersion hydrogen ion implementation and thermal desorption process. Thin Solid Films 485: 135-140.

[111] Pranevicius L, Templier C, Pranevicius LL, Milcius D (2005) Influence of surface barriers on hydrogen storage in MgAl films on permeable stainless steel membranes. Vacuum 78: 367-373.

[112] Liang G, Schulz R (2003) Synthesis of Mg-Ti alloy by mechanical alloying. J. Mater. Sci.38: 1179 – 1184.

IntechOpen